Geophys. J. Int. (1999) **139,** 599–622

Inner core anisotropy inferred by direct inversion of normal mode spectra

Joseph J. Durek* and Barbara Romanowicz
Seismological Laboratory, University of California at Berkeley, 475 *McCone Hall Berkeley,* CA 94720, *USA*

Accepted 1999 May 7. Received 1999 May 5; in original form 1998 July 22

SUMMARY

The spectra of 25 inner-core-sensitive normal modes observed following eight recent major (M_w >7.5) earthquakes are inverted for anisotropic structure in the inner core, using a one-step inversion procedure. The mode data are combined with *PKP*(DF)–*PKP*(AB) differential traveltime data and the inner core is parametrized in terms of general axisymmetric anisotropy, allowing structure beyond restrictive transversely isotropic models with radially varying strength. The models obtained are in good agreement with previous ones derived through the intermediate step of computing splitting functions. Splitting functions predicted for the inner core model determined using the one-step, direct inversion of all mode spectra agree well with those obtained from non-linear inversion of individual modes. We discuss the importance of handling the perturbation to radial isotropic structure appropriately in order to align the observed and predicted spectra properly. We examine the effect of using existing tomographic mantle models to correct for mantle effects on the inner core modes versus a mantle model derived by us using a relatively small number of mantle-sensitive modes, and show that the latter leads to a significantly better fit to the inner core data. Our ability to fit the inner core spectral data degrades appreciably if an isotropic layer thicker than 100–200 km is imposed at the top of the inner core.

Key words: anisotropy, inner core, inversion, normal modes, traveltimes.

INTRODUCTION

Normal mode spectra have been used extensively to constrain long-wavelength three-dimensional structure in the Earth's mantle as well as anisotropy in the inner core (e.g. Woodhouse *et al.* 1986; Ritzwoller *et al.* 1986, 1988; Smith & Masters 1989; Li *et al.* 1991; Widmer *et al.* 1992; Tromp 1995a; Romanowicz *et al.* 1996).

The spectra of modes sensitive only to mantle structure are rather well explained by existing models of elastic heterogeneity based on surface wave and body wave data (e.g. Smith & Masters 1989; Li *et al.* 1991; He & Tromp 1996). In contrast, modes with inner core sensitivity often exhibit splitting, after correction for ellipticity and rotation effects, which significantly exceeds that predicted by mantle models (e.g. Masters & Gilbert 1981; Giardini *et al.* 1988; Widmer *et al.* 1992). This splitting cannot be explained by reasonable isotropic heterogeneity in the mantle or core (e.g. Widmer *et al.* 1992), but has been shown to be consistent with simple axisymmetric models of anisotropy (e.g. Woodhouse *et al.* 1986; Tromp 1993). The dominance of zonal structure observed in these modes is, to a first approximation, well described by transverse isotropy with a symmetry axis parallel to the Earth's rotation axis, as are *PKIKP* traveltime observations, for which paths parallel to the rotation axis are systematically faster than equatorial paths (Poupinet *et al.* 1983; Morelli *et al.* 1986). More recent studies demonstrate complexities in the inner core anisotropic structure beyond simple transverse isotropy (Li *et al.* 1991; Su & Dziewonski 1995; Romanowicz *et al.* 1996; Creager 1997; Souriau & Romanowicz 1997; Tanaka & Hamaguchi 1997).

The occurrence of several major earthquakes since 1994 has provided numerous high-quality digital data owing to the recent global expansion of broad-band digital seismic networks. These data essentially supersede previous normal mode data sets acquired over the last 20 years, and may be used to improve constraints on inner core structure. Using such data, Tromp (1995a) confirmed that a radially varying model of transverse isotropy with a constant axis direction is able to explain a significant fraction of the inner core mode splitting. Romanowicz *et al.* (1996) inverted the splitting functions of 19 inner-core-sensitive modes for axisymmetric models of anisotropy, thus allowing a departure from the radially symmetrical, constant-direction transversely isotropic models commonly

* Now at: SRI International, 333 Ravenswood Avenue, Menlo Park, CA 94025, USA. E-mail: jdurek@unix.sri.com

investigated. One of the main results of their study is that, when relaxing the constraint of radial symmetry, models are obtained in which the region of fast velocities experienced by polar-parallel P waves in the centre of the core is elongated in the direction of the rotation axis. Romanowicz *et al.* (1996) also demonstrated that this class of structure predicts the character of the scatter in traveltime data seen by Song & Helmberger (1995) and is suggestive of long-wavelength convection in the inner core, with flow alignment of hcp-iron crystals as a proposed source for the anisotropy.

Previous normal mode studies investigated the effect of heterogeneity on observed spectra using a two-step procedure in which data for each mode are first inverted for a 'splitting function', describing the depth-averaged effect of lateral heterogeneity in a manner similar to 2-D phase velocity maps in the case of surface waves (e.g. Woodhouse *et al.* 1986; Ritzwoller *et al.* 1988; Giardini *et al.* 1988; Li *et al.* 1991; Resovsky & Ritzwoller 1995, 1998; He & Tromp 1996; Romanowicz *et al.* 1996). The splitting functions for a collection of modes, each with different depth sensitivity, are then inverted jointly in a linear inversion for 3-D elastic and/or anisotropic structure. (e.g. Woodhouse *et al.* 1986; Ritzwoller *et al.* 1988; Li *et al.* 1991; Tromp 1993; Romanowicz *et al.* 1996).

The drawback of the two-step inversion for inner core anisotropy is that the splitting functions inferred for inner-core-sensitive modes depend on the starting model (e.g. Megnin & Romanowicz 1995). The splitting functions thus obtained for each mode may not always be consistent with realistic earth structure (see Li *et al.* 1991 for a discussion).

The success of the two-step inversion is dependent on the uniqueness of the intermediate splitting functions. To avoid potential model errors introduced by non-unique splitting functions, we here perform a direct inversion of the spectra of inner-core-sensitive modes, an approach first introduced by Li *et al.* (1991) and later applied by Tromp (1996) to mantle-sensitive modes. We consider different parametrizations for inner core anisotropy, and different ways to correct for mantle effects. For comparison, from the models thus obtained we compute synthetic splitting functions for these modes and discuss their consistency with splitting functions derived from the data.

THEORETICAL BACKGROUND

In this section, we review the basic theory relating observed spectra of an isolated multiplet to departures from a 1-D reference earth model (PREM; Dziewonski & Anderson 1981). While it is possible also to consider coupled modes (Resovsky & Ritzwoller 1995, 1998; Tromp 1996; Kuo *et al.* 1997), we here consider only the theoretical behaviour of isolated modes. The displacement eigenfunction for a given singlet m in a multiplet of angular order l can be written (Gilbert & Dziewonski 1975)

$$
\begin{aligned}
{}_n u_l^m(\theta, \phi) &= U_n^l(r) Y_l^m(\theta, \phi) + V_n^l(r) \nabla_h Y_l^m(\theta, \phi) \quad \text{(spheroidal)} \quad (1)\\
&= W_n^l(r) \nabla_h \times Y_l^m(\theta, \phi) \quad \text{(toroidal)},
\end{aligned}
$$

where n denotes the radial order of the mode, l defines the angular order, and $-l < m < l$ defines the azimuthal order. In the spherical reference earth model, the $2l+1$ singlets of a multiplet all oscillate at the same frequency.

We represent the internal structure of the earth using lateral and radial basis functions:

$$\delta m(r, \theta, \phi) = \sum_{s,t,k} \delta m_{st}^k P_k(r) Y_s^t(\theta, \phi), \quad (2)$$

where $\delta \mathbf{m} = (\delta\alpha/\alpha, \delta\beta/\beta, \delta\rho/\rho)$ represents perturbations to P velocity, S velocity and density, respectively. Using first-order degenerate perturbation theory, appropriate in the case of isolated multiplets (Dahlen 1969; Woodhouse & Dahlen 1978), the displacement corresponding to a single multiplet of order l can be written in matrix form:

$$\mathbf{u}(t) = \mathcal{Re}\{\exp(i\omega t)\mathbf{r} \cdot \exp(i\mathbf{H}t) \cdot \mathbf{s}\}, \quad (3)$$

where $\mathbf{r}$ and $\mathbf{s}$ are the source and receiver vectors of dimension $2l+1$ that describe the excitation and receiver response of the individual singlets. For this discussion, we ignore the ellipticity and rotation terms, which can be accurately computed (e.g. Dahlen 1968). The effect of heterogeneity on the observed spectra is then fully described by the splitting matrix $\mathbf{H}$, which describes the interaction of two singlets, m and m':

$$H_{mm'} = \omega_o \sum_{s=0}^{s=2l} \sum_{t=-s}^{t=+s} \gamma_{ls}^{mm't} c_s^t, \quad (4)$$

where γ is expressed in terms of 3-j symbols and includes selection rules for singlet interaction through a component of structure, (s, t). The splitting coefficients, c_s^t, are linearly related to the perturbation in structure as follows (Woodhouse *et al.* 1986):

$$c_s^t = \int_0^a \sum_k \delta m_{st}^k P_k(r) M_s(r)\, dr + \sum_d \delta h_{st}^s H_s^d, \quad (5)$$

where the radial sensitivities, $M_s(r)$, to perturbations in velocity and density are given by Li *et al.* (1991).

Following Li *et al.* (1991), the splitting matrix for an anisotropic medium may in turn be written as

$$H_{mm'} = \frac{1}{2\omega_0} \int [\nabla \mathbf{u}_{m'} : \boldsymbol{L}(r, \theta, \phi) : \nabla \mathbf{u}_m^*]\, dV, \quad (6)$$

where $\boldsymbol{L}$ is the fourth-rank elastic tensor with 21 independent components and $\mathbf{u}_m$ is the displacement eigenfunction for the mth singlet. The fourth-rank elastic tensor may be expanded in generalized spherical harmonics:

$$\boldsymbol{L} = \sum_{\alpha\beta\gamma\delta} \sum_{s=0}^{\infty} \sum_{t=-s}^{+s} L_{st}^{\alpha\beta\gamma\delta} Y_s^{Nt}\, \mathbf{e}_\alpha \mathbf{e}_\beta \mathbf{e}_\gamma \mathbf{e}_\delta, \quad (7)$$

where $L_{st}(r)$ are the (radially varying) coefficients of the expansion $N = \alpha + \beta + \gamma + \delta$, where $\alpha, \beta, \gamma, \delta$ take the values -1, 0, 1, $\mathbf{e}_\alpha$ are complex basis vectors and Y_s^{Nt} are the generalized spherical harmonics (Phinney & Burridge 1973). By substituting (7) into (6), the splitting matrix is reduced to a form similar to (4):

$$H_{mm'} = \frac{1}{2\omega_0} \sum_{\substack{s=0\\ even}}^{2l} \sum_{t=-s}^{s} \gamma_{st}^{mm'} \left\{ \sum_{\alpha\beta\gamma\delta} \int_0^a L_{st}^{\alpha\beta\gamma\delta}(r) g_s^{\alpha\beta\gamma\delta} r^2 dr \right\}, \quad (8)$$

where g comprises sensitivity kernels and interaction rules, given explicitly in Li *et al.* (1991). In the case of an isolated multiplet, the coefficients of the expansion of the elastic tensor with s odd do not contribute to the splitting. The term in brackets is the splitting coefficient, c_{st}, in which the contribution of general anisotropy requires summation over all elastic tensor elements. As demonstrated in Li *et al.* (1991), because of symmetry considerations, there are only 13 independent elements for each harmonic component (s, t). For $s=0$ and $s=2$, these numbers reduce to 5 and 11 respectively, since $|\alpha+\beta+\gamma+\delta|\le s$.

Partial derivatives

In the two-step inversion, the splitting coefficients c_{st} for each mode are first iteratively estimated from the observed seismograms $u(t)$. The coefficients for all of the modes are then combined in a linear inversion for intrinsic structure. Following Giardini *et al.* (1988), the linearized partial derivative relating the observations to the splitting coefficients can be deduced by considering the perturbed initial value problem,

$$\frac{d}{dt}\,\delta\boldsymbol{P}=i\delta\boldsymbol{H}\,\boldsymbol{P}+i\boldsymbol{H}\,\delta\boldsymbol{P}\,,\quad \delta\boldsymbol{P}(0)=0\,, \tag{9}$$

which has the solution

$$\delta\boldsymbol{P}=\int_0^t \boldsymbol{P}(t-t')\delta\boldsymbol{H}\boldsymbol{P}(t')\,dt'\,. \tag{10}$$

The solution, $\boldsymbol{P}(t)=\exp(i\boldsymbol{H}t)$, to the unperturbed problem can be decomposed using the eigenvectors $\mathbf{U}$ and eigenvalues $\boldsymbol{\Omega}$ of the splitting matrix $\boldsymbol{H}$:

$$\boldsymbol{P}(t)=\mathbf{U}\exp(i\boldsymbol{\Omega}t)\mathbf{U}^{-1}\,. \tag{11}$$

Substituting into eq. (11), the solution takes the form

$$\delta P_{ij}=\sum_{pqmm'}\int_0^t iU_{ip}\exp[i\Omega_{pp}(t-t')] \times U^{-1}_{pm}\delta H_{mm'}U_{m'q}\exp[i\Omega_{qq}t']U^{-1}_{qj}\,. \tag{12}$$

Integration over time provides a linear relationship between the perturbation in $\boldsymbol{P}(t)$ in eq. (3) and a perturbation in the splitting matrix,

$$\frac{\partial\exp(i\boldsymbol{H}t)}{\partial H_{mm'}}=\sum_{pq}U_{ip}U^{-1}_{pm}U_{m'q}U^{-1}_{qj}\,\frac{e^{i\Omega_{qq}t}-e^{i\Omega_{pp}t}}{\Omega_{qq}-\Omega_{pp}}\,,\quad p\ne q\,. \tag{13}$$

From the relationship between the splitting matrix and the splitting coefficients (eq. 4), the linearized seismogram can be written in the form

$$\delta u(t)=\mathscr{Re}\left(\sum_{pqst}\omega_0 r'_p s'_q \gamma'_{pqst}\,\frac{e^{i\Omega_{qq}t}-e^{i\Omega_{pp}t}}{\Omega_{qq}-\Omega_{pp}}\,\delta c_{st}\right),\quad p\ne q\,, \tag{14}$$

leading to the ability to evaluate the partial derivative $\partial u(t)/\partial c_{st}$.

Since the relationship between each splitting coefficient and intrinsic structure in eq. (5) is linear, the partial derivative to infer structure from the splitting coefficients $\partial c_{st}/\partial m^k_{st}$ is easily formed.

In the direct inversion, we simply combine the two partial derivatives discussed above to generate the linearized derivative relating the observed seismogram directly to intrinsic structure, $\partial u(t)/\partial m^k_{st}$.

DATA SELECTION AND PREPARATION

We consider data from eight large earthquakes ($7.5<M_w<8.0$) since 1994 (Table 1). Four of these events have intermediate-to-deep foci, providing good excitation of deep sampling overtones and in particular of inner-core-sensitive modes. Each of these events was recorded at more than 100 three-component broad-band stations distributed over the globe.

Since we are particularly interested in spheroidal modes that sample into the inner core, we only consider vertical-component records, which have the best signal/noise ratio. The data are processed as follows.

(1) Raw time-series are extracted, starting 10–20 hr before the event and roughly 100–200 hr following the event.

(2) Obvious glitches are removed. Single-sample spikes are interpolated, while data gaps, which are considerably more rare than in data sets used in earlier normal mode studies, are flagged or rejected.

(3) All frequencies below 0.05 mHz are removed using a polynomial fitting scheme (flagged data gaps are ignored).

(4) The time-series are reduced to acceleration and are compared to synthetic seismograms to detect errors in the reported instrument response.

(5) Additional editing is performed to remove subsequent events or aftershocks.

The presence of large events following the main event of interest introduces two corrupting influences. First, they excite low-Q modes, effectively elevating the noise floor. Second, if sufficiently large, they modify the phase and amplitude of the mode of interest. While the first problem is largely addressed by windowing out several hours following the aftershock, the second problem requires including the perturbing effect of the aftershock in the inversion. For the time windows used in this study, we have modelled the effect of subsequent events and found it to be negligible.

Table 1. Earthquakes used in the analysis.

Centroid time			Centroid hypocentre						Moment tensor elements ($\times 10^{20}$ N m)					
Date	Time	Region	Lat.	Long.	Depth	Duration	M_w	M_o (10^{20} N m)	M_{rr}	$M_{\theta\theta}$	$M_{\phi\phi}$	$M_{r\theta}$	$M_{r\phi}$	$M_{\theta\phi}$
1996 Jan 01	08:05:23.1	Minahassa Peninsula	0.74	119.93	15	44.0	7.9	7.78	1.35	−0.99	−0.36	−7.27	−2.36	−0.86
1996 Feb 17	06:00:02.7	West Irian Region	−0.67	136.62	15	59.2	8.2	24.10	8.48	−7.15	−1.33	−18.31	13.13	3.10
1994 Mar 09	23:28:17.7	Fiji Islands Region	−17.69	−178.11	568	32.0	7.6	3.07	−1.22	0.20	1.02	−0.13	−2.50	1.39
1994 Jun 09	00:33:45.4	Northern Bolivia	−13.83	−67.56	647	40.0	8.2	26.30	−7.59	7.75	−0.16	−25.03	0.42	−2.48
1996 Jun 17	11:22:33.7	Flores Sea	−7.38	123.02	584	38.8	7.8	7.30	−5.53	6.01	−0.48	−1.59	3.43	2.48
1995 Jul 30	05:11:23.5	Northern Chile	−24.17	−70.74	29	32.0	8.0	12.15	8.26	0.43	−8.69	0.30	−8.67	0.64
1994 Oct 04	13:23:28.5	Kuril Islands	43.60	147.63	69	50.0	8.3	30.00	12.14	10.87	−23.01	17.82	9.80	−9.39
1995 Oct 09	15:36:28.8	Jalisco, Mexico	19.34	−104.80	15	38.8	8.0	11.47	3.62	−2.53	−1.09	9.44	−5.49	1.40

To edit the data for individual modes, the time-series are Hann-tapered and transformed to the spectral domain. For each station, the time window is specified that visually provides the best signal-to-noise ratio in the spectral domain and presents the least interference with other modes. The time window chosen is generally 1.0–1.7 Q-cycles in length, a range determined by Dahlen (1982) to optimize the trade-off between signal loss and spectral resolution for a Hann-tapered record. Synthetic seismograms are generated during editing for two purposes: to assess the consistency of predictions from existing 3-D models, and to examine the excitation of the target multiplet relative to neighbouring modes. Each synthetic trace is generated in the time domain, and the same windowing, filtering and processing as for the data are applied.

Inner-core-sensitive multiplets are examined that are isolated from neighbouring multiplets, resulting from separation in either frequency or quality factor. Since inner-core-sensitive modes are typically characterized by slow decay, a time window may be chosen after an event such that low-Q neighbouring modes have decayed into the noise. For several of the modes studied, it is necessary to start the time window for spectral analysis roughly 5–20 hr following the event to allow well-excited neighbouring low-Q modes to decay into the noise.

We assume source parameters as given in the CMT catalogue (Dziewonski *et al.* 1981). To account for the source duration of these large events, which becomes a significant fraction of the mode period at the shortest periods ($T \sim 100$ s), we convolve the predicted trace with a boxcar with the width of the source duration. We assume that the complexity of the source rupture is a second-order effect. The consequence of neglecting the temporal extent of rupture for these large events is an underestimation of the quality factor by 3–5 per cent for modes between 100 and 200 s period, decreasing to no effect at the longest periods. This systematic bias is due to the fact that a seismogram that is not convolved with the source duration will overpredict the short-period energy and thus require greater attenuation (lower Q) to match the data.

DETERMINATION OF SPLITTING FUNCTIONS

In this section, we document the effect of heterogeneity on normal mode spectra by inverting for the splitting function of each mode (eqs 4 and 14). We later assess the consistency of the retrieved splitting functions with those predicted from inner core structure obtained from a one-step inversion of all mode observations.

The objective function to be minimized is a combination of the misfit to the data as well as some property of the model, m:

$$\Phi(m) = [d - f(m)]^{\mathrm{T}} C_e^{-1} [d - f(m)] + m^{\mathrm{T}} C_m^{-1} m \,. \tag{15}$$

In our application, d represents the observed complex spectrum for a mode at all stations and f is the non-linear relation between the desired splitting functions, m, and the spectrum of each mode. The data covariance matrix, C_e, essentially weights the data by the inverse of its uncertainty and assures uniform variance. There are numerous schemes to approximate accurately this matrix in applications where it is difficult to assess all data errors. Among these are weighting the data by the *a posteriori* misfit (Wong 1989; He & Tromp 1996) and assessing the signal-to-noise ratio using a window prior to each event (Li *et al.* 1991). We implement the following weighting scheme, the two parts of which must be combined to give a balanced weighting of the data. First, for each event we normalize the average variance of each event. Thus, data randomly chosen from two events will have roughly the same contribution to the inversion. However, data from different stations within an event will be weighted only by their natural amplitude, since we do not want to boost the contribution of nodal stations artificially. For the second part of the weight, we assign a qualitative grade based on the noise level, the strength of neighbouring modes, and the significance of the particular record to constrain the final solution. While we could explicitly calculate a signal-to-noise level using a noise sample preceding the earthquake, we believe that this quality grade allows greater flexibility in assessing shortcomings in the data.

The model covariance matrix, C_m, imposes prior restrictions on the solution space of possible models, and often enforces an *a priori* assumption about how the model should behave. In this implementation, we apply a damping on both the model norm and the gradient.

While the uncertainties in the retrieved splitting functions may be evaluated using the *a posteriori* model covariance matrix, C_m, we have instead investigated the robustness of the models using a bootstrap method. A quarter of the data for each mode are randomly selected and inverted for a splitting function, with damping modified to preserve the same number of degrees of freedom as in the inversion of the full data set. The variability of the retrieved coefficients indicates its importance in explaining the observed spectra and is taken as a measure of the uncertainty. While the statistics of the bootstrap method are strictly valid only when the data are all independent, we argue that this method provides a measure of the relative uncertainties amongst the coefficients for each mode, although the absolute level of error may be less well estimated.

The availability of data from several earthquakes and the balanced weighting of the data lead to convergence within 3–4 iterations. After the first couple of iterations, in which the solution is in the neighbourhood of a minimum, we allow the moment of each event to be adjusted to correct for source error.

Fig. 1 demonstrates the success of describing the observed spectra through an inverse procedure for the splitting coefficients.

Starting model

For modes sensitive to the mantle only, it is our experience that the splitting function obtained from the non-linear iterative inversion is independent of the (reasonable) starting model (e.g. Li *et al.* 1991; Kuo *et al.* 1997). For the core-sensitive modes, whose strong splitting represents the largest observed departure from sphericity, the retrieved splitting function is dependent on the starting model, and convergence with meaningful variance reduction is not often obtained when starting from PREM. Megnin & Romanowicz (1995) have demonstrated that the solution spaces for several core-sensitive modes have numerous local minima and, for some modes such as ${}_{13}S_2$, multiple global minima (although in such cases the alternative solutions are generally inconsistent with solutions from other modes or *a priori* constraints on model size). We choose starting models based on combinations of existing mantle models (e.g. SAW12D, Li & Romanowicz 1996) and existing models of inner core anisotropy (SAT, Li *et al.* 1991; STO, Shearer *et al.* 1988; CRG, Creager 1992). In several cases,

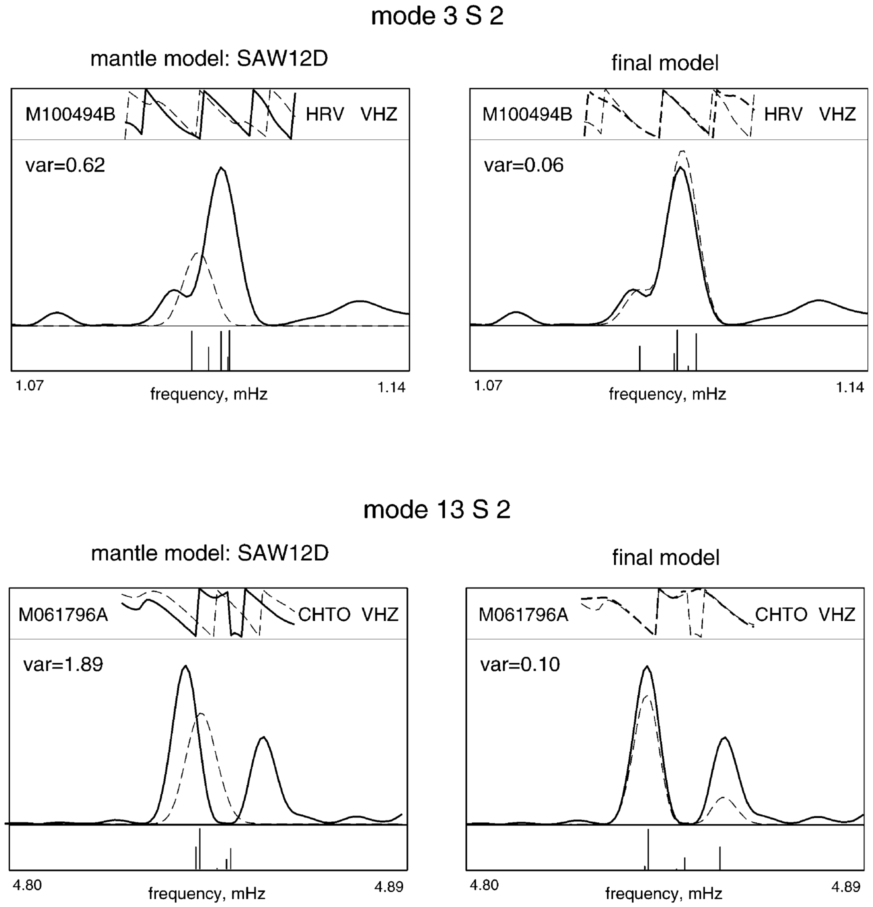

Figure 1. Each frame compares the normal mode phase (top) and amplitude (bottom) spectra that are observed (solid) and predicted (dashed). The predictions of the retrieved splitting functions (right) are significantly improved compared to those based only on mantle structure, ellipticity and rotation (left).

the convergence behaviour is significantly improved if we first invert for degree 0 splitting coefficients (perturbation in centre frequency and Q of the mode) and incorporate these shifts into the starting solution. In addition, several diagnostics exist that are useful in discriminating between two competing solutions: (1) limited variance reduction and poor convergence, (2) significant misfit to a subset of data, and (3) large decrease in moment adjustment for a specific event, indicating that data from an event are inconsistent with the solution.

As an example, Fig. 2 presents two competing splitting functions for ${}_{13}S_2$ obtained using different starting models that fit the data to a similar level. To help discriminate between the two solutions, Fig. 3 compares the amplitude spectrum predictions of the two splitting functions with the observations for a great event in the Flores Sea (06/17/96). While both retrieved splitting functions have some difficulty at high latitudes, solution B completely fails to predict an obvious singlet visible at mid-latitude stations and predicts a singlet not visible in the data. These failures allow us to reject the bottom splitting function as not adequate to explain the data.

Impact of short-wavelength structure

Each isolated mode is sensitive to lateral structure up to angular order $2l$, where l is the angular order of the mode. Thus, several of the modes considered have no sensitivity beyond degree 6, the truncation level in this study, and are not subject to aliasing effects, a great advantage of normal mode analysis. However, we can also make the argument that low-degree structure is a dominant component of the observed splitting. The core-sensitive modes of angular orders 1 and 2 (sensitive only to structure up to degrees 2 and 4 respectively) are among the modes most anomalously split. The distribution of singlet frequencies for observed spectra also shows a dominant signal related to degree 2 structure (Widmer *et al.* 1992).

For two sample modes sensitive to higher-order structure, ${}_{11}S_5$ and ${}_8S_5$, we have compared solutions when we increase the truncation of the spherical harmonic expansion beyond the degree 6 used in the final solutions. Both modes are sensitive to structure at degree 10 ($s=2l$). In Fig. 4(a), the power spectrum of the splitting function for mode ${}_8S_5$ clearly shows that structure through degree 6 remains largely unchanged as the truncation level is extended to higher degrees. The correlation at all degrees is significant beyond the 98 per cent level. It is also clear that the amplitude in degree 4 decreases by 30 per cent as the truncation is extended to degree 6, suggesting that truncation at degree 4 introduces aliasing. A statistical F-test shows that the extension of the inversion to degree 6 is significant beyond the 90 per cent level, while the variance reduction gained from truncations at degrees 8 and 10 are unjustified. Mode ${}_{11}S_5$ (Fig. 4b) illustrates this further, in that the amplitude

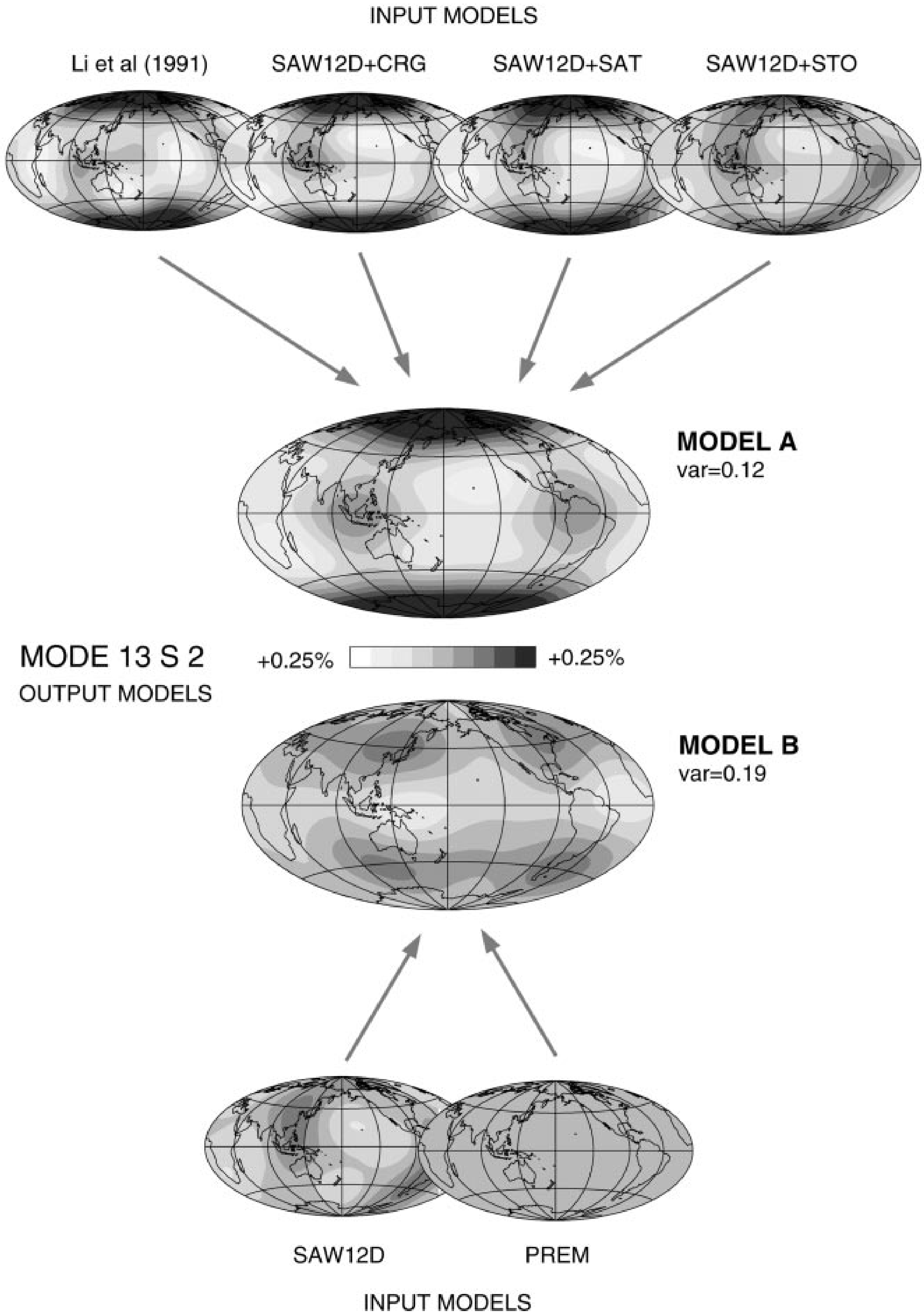

Figure 2. Comparison of two alternative splitting functions (centre) for mode ${}_{13}S_2$ retrieved from different starting models.

in degree 4 changes by up to 40 per cent as the truncation is extended beyond degree 6, and the F-test also justifies the additional structure. However, we again find that the pattern represented by degrees 2–6 is spatially stable (correlation beyond 98 per cent significance), and question the accuracy of the structure at degree 10 given that roughly 300 independent data are constraining 67 harmonic coefficients.

Splitting functions of inner core modes

We applied the non-linear iterative inversion to 25 inner-core-sensitive modes, ${}_3S_2$, ${}_5S_2$, ${}_5S_3$, ${}_8S_1$, ${}_8S_5$, ${}_9S_2$, ${}_9S_3$, ${}_9S_4$, ${}_{11}S_4$, ${}_{11}S_5$, ${}_{13}S_1$, ${}_{13}S_2$, ${}_{13}S_3$, ${}_{14}S_4$, ${}_{15}S_3$, ${}_{16}S_5$, ${}_{18}S_2$, ${}_{18}S_3$, ${}_{18}S_4$, ${}_{21}S_6$, ${}_{22}S_1$, ${}_{23}S_4$, ${}_{23}S_5$, ${}_{27}S_1$, ${}_{27}S_2$. Table 2 presents the distribution of shear and compressional energy of these modes in the inner core.

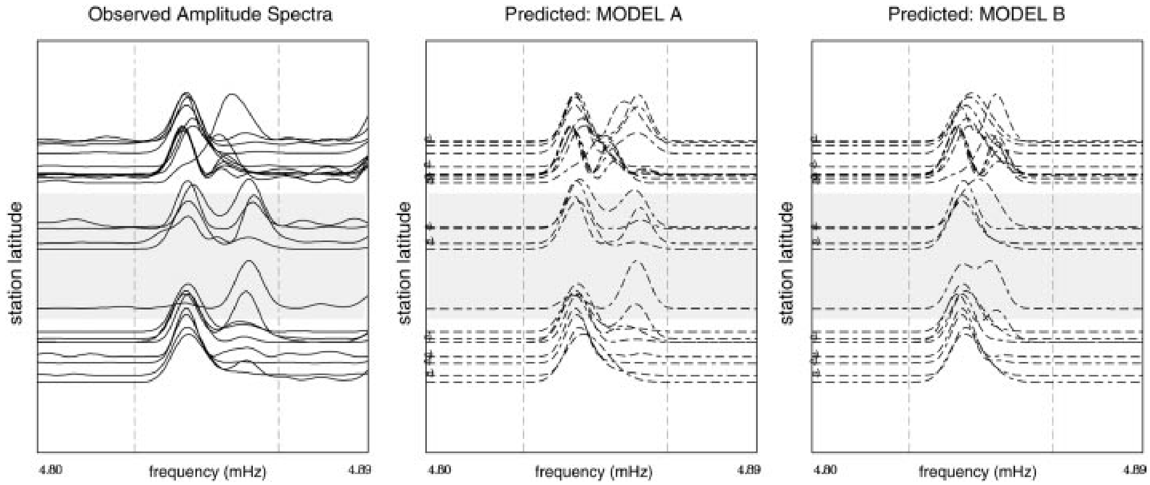

Figure 3. Comparison of the observed amplitude spectra (left) of mode ${}_{13}S_2$ with those predicted for the two retrieved splitting functions (Fig. 2). While the variance reduction to the total data set is similar, model 'B' exhibits difficulty in explaining observations near the equator.

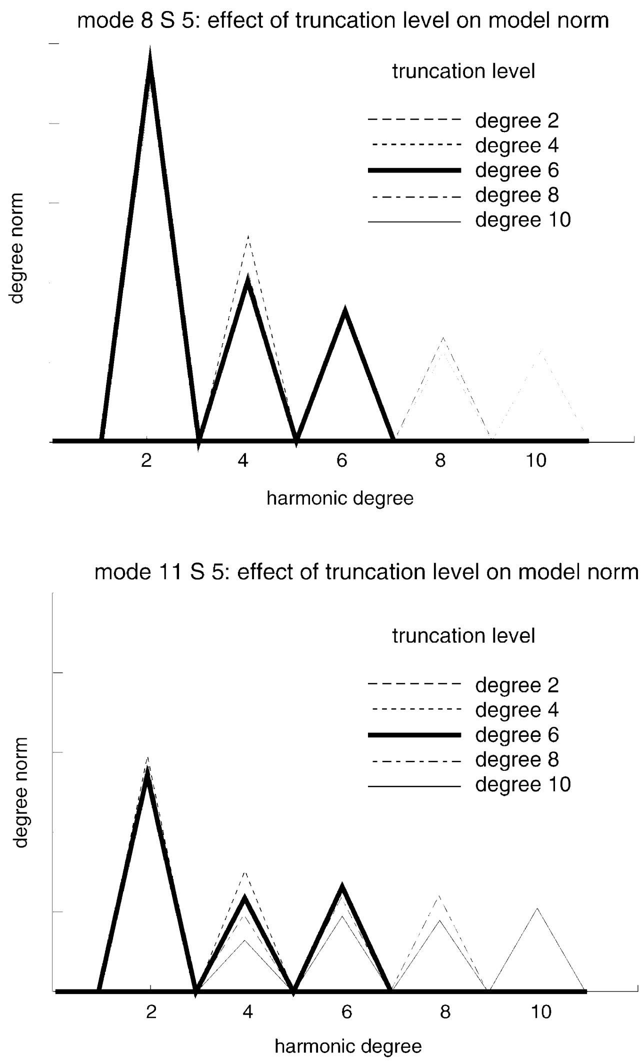

Figure 4. The normalized amplitude in each degree for splitting functions retrieved with different truncation levels: (top) mode ${}_8S_5$, (bottom) mode ${}_{11}S_5$.

Table 2. Energy density of inner-core-sensitive modes.

Mode	Percentage of energy in core			
	Outer	Inner		
		Total	Bulk	Shear
${}_3S_2$	22.1	7.7	0.1	7.6
${}_5S_2$	20.1	0.5	0.0	0.5
${}_5S_3$	16.8	0.2	0.0	0.2
${}_8S_1$	44.7	7.7	6.7	1.0
${}_8S_5$	38.1	2.8	0.0	2.8
${}_9S_2$	15.1	0.9	0.6	0.3
${}_9S_3$	42.6	0.9	0.6	0.3
${}_9S_4$	39.0	7.3	0.2	7.1
${}_{11}S_4$	47.4	1.4	0.2	1.2
${}_{11}S_5$	45.1	0.8	0.1	0.7
${}_{13}S_1$	37.0	18.3	15.5	2.8
${}_{13}S_2$	43.3	9.6	8.3	1.3
${}_{13}S_3$	47.3	4.5	3.4	1.1
${}_{14}S_4$	46.8	4.9	1.2	3.7
${}_{15}S_3$	47.7	8.8	7.2	1.6
${}_{16}S_5$	43.0	1.8	0.7	1.2
${}_{18}S_2$	32.3	15.2	12.6	2.6
${}_{18}S_3$	41.7	11.4	9.8	1.6
${}_{18}S_4$	44.8	6.0	5.0	1.0
${}_{21}S_6$	46.1	2.7	1.4	1.3
${}_{22}S_1$	42.9	15.9	12.4	3.5
${}_{23}S_4$	41.1	13.0	10.8	2.2
${}_{23}S_5$	45.1	7.9	6.7	1.2
${}_{27}S_1$	37.3	20.1	15.5	4.7
${}_{27}S_2$	42.4	14.7	12.4	2.3

We did not include the following modes due to their overlap and potential coupling with other modes: ${}_2S_3$, ${}_3S_1$, ${}_6S_3$, ${}_7S_2$. While Resovsky & Ritzwoller (1995) demonstrated that, even in the case of significant coupling between two modes, the degree 2 splitting function is largely unbiased, we will avoid such complications in this analysis.

Table 3 presents the variance reduction, resolution and splitting width resulting from the inversions for the splitting coefficients of 25 modes. Modes ${}_5S_2$, ${}_5S_3$ and ${}_9S_2$ would not be classified as anomalously split, as might be expected since these modes have little sensitivity to the inner core.

Table 3. Results of splitting function inversion. The variance ratio is defined as the squared misfit relative to the squared data. The initial variance (Var_0) is obtained using ellipticity, rotation and mantle model SAW12D and is compared with that obtained following inversion for the splitting functions of each mode. The splitting width, W, in the frequency spread of the $2l+1$ singlets is compared with that predicted for rotation, ellipticity and mantle model SAW12D (Li & Romanowicz 1996). The degrees of freedom (R) is the trace of the resolution matrix given relative to the number of unknowns describing lateral structure.

Mode	Var_0	Var	W	R	# records
${}_3S_2$	1.343	0.209	1.49	11.5/14	103
${}_5S_2$	0.414	0.070	1.16	5.4/14	34
${}_5S_3$	0.221	0.126	1.08	17.6/27	81
${}_8S_1$	0.864	0.187	1.42	6.9/7	119
${}_8S_5$	1.129	0.223	1.91	24.1/26	131
${}_9S_2$	0.675	0.266	1.23	12.0/14	61
${}_9S_3$	1.323	0.187	1.57	21.0/26	89
${}_9S_4$	1.365	0.235	2.26	17.3/26	59
${}_{11}S_4$	1.166	0.074	1.80	21.3/27	117
${}_{11}S_5$	0.607	0.124	1.41	22.7/27	113
${}_{13}S_1$	3.291	0.250	2.37	6.5/7	90
${}_{13}S_2$	1.173	0.123	2.15	12.1/14	104
${}_{13}S_3$	1.035	0.166	1.53	23.8/27	121
${}_{14}S_4$	1.869	0.239	1.56	14.8/27	46
${}_{15}S_3$	1.438	0.229	1.66	16.0/27	102
${}_{16}S_5$	2.378	0.165	1.59	17.4/27	70
${}_{18}S_2$	2.621	0.343	1.95	9.6/14	54
${}_{18}S_3$	2.702	0.266	1.39	17.6/27	90
${}_{18}S_4$	0.871	0.176	1.42	19.4/27	120
${}_{21}S_6$	2.414	0.305	1.41	14.1/27	64
${}_{22}S_1$	0.609	0.188	1.65	6.2/7	47
${}_{23}S_4$	1.892	0.279	1.56	15.8/27	81
${}_{23}S_5$	1.424	0.251	1.35	12.3/27	91
${}_{27}S_1$	1.146	0.477	1.38	5.7/7	41
${}_{27}S_2$	1.195	0.259	1.66	11.5/14	97

The degree 0 coefficients of the splitting functions represent the corrections to the reference model, in centre frequency and attenuation, presented in Table 4. Many of the adjustments of the modes relative to PREM are in the same direction, if not of a similar magnitude to those presented by Li *et al.* (1991) Widmer *et al.*(1992), and He & Tromp (1996).

The splitting function coefficients, their uncertainties and resolution are presented in Table 5, with corresponding splitting functions plotted in Fig. 5. While the mantle contribution to most of these modes is dominated by a c_{22} structure associated with subduction, the splitting functions are generally dominated by an anomalously large zonal structure. To demonstrate this, Figs 6 and 7 respectively compare the zonal c_{20} and c_{40} coefficients with those predicted for a typical mantle model (SAW12D, Li & Romanowicz 1996) as well as coefficients from other published studies.

To reiterate the relationship between the observed splitting and possible anisotropic structure in the inner core, Fig. 8 compares the c_{20} and c_{40} coefficients of each mode, corrected for mantle structure, with the rms values of the anisotropic kernels for each degree s (Woodhouse *et al.* 1986) under the restrictive assumption that the anisotropy is transversely isotropic. For both degrees 2 and 4, the outlying point is the coefficient for mode ${}_3S_2$, indicating the large splitting and high sensitivity to inner core anisotropy documented by Woodhouse *et al.* (1986). It may be argued that a linear trend relating observed splitting

Table 4. Centre frequencies and quality factors for inner-core-sensitive modes.

Mode	Centre frequency		Quality factor	
	PREM	Observed	PREM	Observed
${}_3S_2$	1106.21	1106.02±0.12	366	334±12
${}_5S_2$	2091.27	2090.81±0.17	317	364±10
${}_5S_3$	2169.66	2168.76±0.10	292	335±8
${}_8S_1$	2873.36	2872.65±0.04	929	1044±17
${}_8S_5$	4166.20	4165.41±0.09	611	708±9
${}_9S_2$	3231.73	3231.10±0.25	407	496±13
${}_9S_3$	3554.98	3556.62±0.14	777	744±17
${}_9S_4$	3877.96	3879.88±0.38	515	564±18
${}_{11}S_4$	4766.87	4766.16±0.06	701	742±8
${}_{11}S_5$	5074.41	5072.95±0.10	665	676±11
${}_{13}S_1$	4495.73	4494.51±0.05	735	691±7
${}_{13}S_2$	4845.26	4844.63±0.04	878	944±11
${}_{13}S_3$	5193.82	5194.01±0.07	908	1009±13
${}_{14}S_4$	5541.84	5542.66±0.33	742	759±21
${}_{15}S_3$	6035.23	6030.93±0.10	806	816±13
${}_{16}S_5$	6836.40	6830.30±0.14	581	544±7
${}_{18}S_2$	6545.68	6538.69±0.63	533	450±8
${}_{18}S_3$	6891.92	6886.42±0.13	851	858±11
${}_{18}S_4$	7240.99	7238.51±0.09	943	1026±9
${}_{21}S_6$	8850.77	8849.64±0.36	740	583±12
${}_{22}S_1$	7819.55	7822.39±0.12	767	1038±16
${}_{23}S_4$	8941.57	8937.26±0.31	809	825±9
${}_{23}S_5$	9289.58	9289.92±0.14	899	947±10
${}_{27}S_1$	9485.85	9496.15±0.70	648	967±47
${}_{27}S_2$	9865.34	9873.37±0.19	789	874±17

and sensitivity exists for the degree 2 coefficients, suggesting why transverse isotropy has been successful in explaining the dominant character of observed splitting. However, the departures from the linear trend seen for the degree 4 coefficients suggest that additional complexity beyond transverse isotropy is required to explain the data fully.

DIRECT INVERSION OF NORMAL MODE SPECTRA

Since the splitting functions for inner core modes exhibit non-uniqueness with multiple minima (e.g. Li *et al.* 1991; Megnin & Romanowicz 1995), we cannot assert that the splitting functions of all the modes are representative of the Earth's structure. To circumvent this problem, we perform a direct and simultaneous iterative inversion of all observed mode spectra for inner core anisotropy. In such an approach, the spectra of each mode may only be modelled by structures allowed by the model parametrization.

Model parametrization

The anomalous signal in the mode spectra is dominated by zonal structure, as exemplified by the large c_{20} and c_{40} coefficients of the splitting functions. We can thus expect to explain a significant fraction of the anomalous splitting by restricting our investigation to axisymmetric structures, which effectively perturbs only the c_{00}, c_{20} and c_{40} splitting coefficients of each mode. This strong restriction is in contrast to the inversion for individual splitting functions in which 6–28 free parameters were allowed per mode. In the direct inversion of normal mode spectra, we will consider the following heterogeneous structures.

Table 5. Splitting function coefficients with corresponding error and resolution estimates.

Mode	degree 2					degree 4									degree 6												
	A_2^0	A_2^1	B_2^1	A_2^2	B_2^2	A_4^0	A_4^1	B_4^1	A_4^2	B_4^2	A_4^3	B_4^3	A_4^4	B_4^4	A_6^0	A_6^1	B_6^1	A_6^2	B_6^2	A_6^3	B_6^3	A_6^4	B_6^4	A_6^5	B_6^5	A_6^6	B_6^6
	3130	−363	139	−96	−716	−702	−271	101	−553	−72	−361	−65	−13	22													
${}_3S_2$	177	225	118	176	209	236	181	118	166	164	148	179	155	132													
	0.89	0.89	0.91	0.85	0.88	0.72	0.73	0.83	0.77	0.79	0.87	0.87	0.66	0.66													
	418	−11	337	−193	−451	512	125	−11	−31	−9	−106	54	4	23													
${}_5S_2$	53	147	101	103	89	87	73	60	75	59	50	60	47	30													
	0.54	0.65	0.60	0.46	0.53	0.55	0.32	0.39	0.38	0.41	0.16	0.17	0.11	0.10													
	261	−157	234	−465	−700	47	82	−5	52	−4	57	109	−117	101	102	15	−75	−68	−31	170	−187	−33	46	−7	−26	0	
${}_5S_3$	88	72	81	106	94	83	53	81	104	87	81	125	70	70	56	68	65	83	63	60	66	60	63	77	45	44	75
	0.84	0.89	0.89	0.81	0.85	0.75	0.74	0.72	0.55	0.67	0.53	0.67	0.69	0.68	0.54	0.43	0.61	0.59	0.55	0.52	0.61	0.57	0.61	0.63	0.60	0.55	0.46
	404	−24	109	−81	−167																						
${}_8S_1$	13	109	111	19	16																						
	1.00	0.97	0.97	1.00	1.00																						
	1188	−98	246	−108	−453	−268	−57	−235	−303	−188	296	19	−24	115	144	68	−211	−147	200	−14	−164	124	58	−50	67	32	−63
${}_8S_5$	44	60	79	56	71	49	87	123	108	193	113	126	123	87	52	73	83	118	154	123	152	129	73	111	99	57	67
	0.99	0.97	0.98	0.97	0.98	0.97	0.89	0.91	0.80	0.78	0.78	0.78	0.88	0.89	0.92	0.86	0.86	0.72	0.72	0.61	0.65	0.53	0.64	0.66	0.63	0.88	0.85
	392	−69	454	−250	−508	189	30	−18	324	59	−340	37	−200	−80													
${}_9S_2$	95	−164	−192	145	126	127	−110	−87	165	108	−194	−152	155	81													
	0.95	0.89	0.91	0.88	0.90	0.87	0.89	0.93	0.81	0.80	0.79	0.81	0.78	0.78													
	643	−300	233	79	27	−294	−188	−45	19	−12	81	−81	24	53	207	−186	55	−20	−242	75	184	−109	49	61	17	−90	9
${}_9S_3$	290	307	217	375	350	186	165	237	252	273	262	292	269	200	143	185	201	143	169	199	205	212	155	191	185	112	145
	0.95	0.91	0.92	0.90	0.83	0.91	0.80	0.82	0.44	0.51	0.52	0.49	0.68	0.65	0.80	0.75	0.65	0.73	0.76	0.75	0.72	0.61	0.64	0.70	0.69	0.92	0.95
	1688	25	−183	−432	−258	−247	−73	−284	−192	−78	−398	97	184	6	22	43	−39	−26	−136	−1	−16	21	−28	183	115	88	−90
${}_9S_4$	145	139	251	150	145	101	233	138	152	178	140	202	192	196	72	86	104	97	84	107	107	71	66	117	140	92	106
	0.97	0.94	0.93	0.92	0.89	0.84	0.83	0.79	0.52	0.54	0.60	0.48	0.70	0.64	0.41	0.71	0.66	0.52	0.50	0.40	0.37	0.19	0.26	0.43	0.49	0.89	0.89
	1101	3	62	−116	−412	125	−139	−229	80	206	43	−74	−101	−21	−291	−2	14	−52	−124	−22	111	2	−26	−30	105	124	28
${}_{11}S_4$	26	29	34	43	51	29	37	36	61	57	68	66	49	48	44	37	51	43	45	61	78	50	47	51	59	23	17
	0.98	0.98	0.98	0.95	0.96	0.95	0.95	0.94	0.71	0.72	0.75	0.68	0.84	0.80	0.86	0.88	0.83	0.71	0.71	0.60	0.59	0.49	0.52	0.53	0.57	0.92	0.94
	673	−35	162	−155	−307	68	−186	−2	63	38	−172	−137	1	94	−73	−71	−36	9	−149	−55	157	17	59	−94	20	234	−29
${}_{11}S_5$	48	−44	−79	67	57	58	−61	−83	98	66	−114	−113	81	116	78	−57	−55	98	83	−78	−114	103	92	−129	−96	74	53
	0.99	0.99	0.98	0.98	0.97	0.96	0.96	0.95	0.87	0.87	0.84	0.79	0.90	0.88	0.90	0.90	0.87	0.79	0.74	0.67	0.63	0.56	0.69	0.64	0.68	0.83	0.85
	1426	−342	−568	−38	−176																						
${}_{13}S_1$	56	247	175	38	27																						
	0.98	0.77	0.82	0.99	0.99																						
	1053	−78	94	−324	−310	708	−171	−5	106	31	−48	79	42	70													
${}_{13}S_2$	19	54	68	85	101	20	81	71	79	86	55	53	18	21													
	0.98	0.92	0.89	0.85	0.84	0.97	0.74	0.85	0.75	0.77	0.82	0.86	0.98	0.96													
	903	148	21	−203	−154	71	−24	−280	−58	−124	−235	−90	140	100	−126	−84	−132	24	−24	−59	−59	−135	−63	30	−48	37	35
${}_{13}S_3$	30	66	76	81	65	46	78	76	99	97	96	151	101	74	38	27	45	60	71	84	81	73	63	53	57	21	17
	0.99	0.96	0.94	0.96	0.95	0.98	0.91	0.91	0.73	0.74	0.79	0.73	0.82	0.80	0.97	0.96	0.96	0.93	0.91	0.85	0.82	0.81	0.77	0.82	0.84	0.97	0.98
	1071	57	10	−3	81	−343	38	48	−168	−131	86	−19	23	21	−137	−17	127	48	−105	−65	4	−75	287	−87	−155	−193	−27
${}_{14}S_4$	89	103	122	148	166	110	118	68	121	99	159	119	121	158	85	48	68	73	79	87	51	47	84	84	78	85	65
	0.88	0.80	0.82	0.76	0.72	0.78	0.80	0.71	0.42	0.38	0.36	0.38	0.57	0.48	0.69	0.63	0.48	0.38	0.39	0.46	0.44	0.42	0.39	0.37	0.37	0.34	0.61
	653	−211	71	−524	−572	182	92	−106	34	−49	−22	−110	−180	24	−36	−59	−114	−10	20	−45	−1	−139	−13	130	12	154	104
${}_{15}S_3$	50	73	89	68	62	43	50	47	42	34	30	62	46	50	27	45	31	40	30	47	44	35	48	59	34	43	42
	0.90	0.85	0.77	0.75	0.80	0.71	0.57	0.53	0.36	0.33	0.29	0.29	0.57	0.45	0.79	0.71	0.80	0.50	0.65	0.49	0.43	0.46	0.44	0.50	0.46	0.76	0.79
	971	107	191	−208	−562	3	−367	−42	−126	86	−150	−16	−105	−5	67	−200	158	−74	−43	35	−30	−53	84	122	−82	178	−117
${}_{16}S_5$	42	72	63	92	53	63	78	73	91	76	84	98	136	90	79	66	80	76	75	73	58	71	93	63	−80	67	39
	0.96	0.95	0.95	0.92	0.94	0.87	0.78	0.85	0.58	0.61	0.64	0.52	0.71	0.74	0.70	0.69	0.64	0.51	0.54	0.38	0.33	0.26	0.28	0.35	0.40	0.69	0.61

Table 5. (*Continued.*)

Mode	degree 2					degree 4									degree 6												
	A_2^0	A_2^1	B_2^1	A_2^2	B_2^2	A_4^0	A_4^1	B_4^1	A_4^2	B_4^2	A_4^3	B_4^3	A_4^4	B_4^4	A_6^0	A_6^1	B_6^1	A_6^2	B_6^2	A_6^3	B_6^3	A_6^4	B_6^4	A_6^5	B_6^5	A_6^6	B_6^6
	846	−53	122	−142	−228	770	−254	−354	−59	−4	−72	256	−150	−62													
${}_{18}S_2$	112	115	184	144	115	142	107	170	141	98	104	130	109	130													
	0.85	0.76	0.81	0.67	0.70	0.78	0.52	0.70	0.52	0.51	0.59	0.71	0.72	0.72													
	669	8	122	−142	−280	213	−178	−241	−37	−138	−71	−66	170	25	−113	−25	93	−14	−64	−44	114	84	32	−60	−83	111	−69
${}_{18}S_3$	41	97	137	116	122	77	54	133	68	84	78	76	45	59	58	89	73	51	73	85	79	27	62	56	37	30	30
	0.96	0.86	0.88	0.80	0.74	0.91	0.71	0.66	0.34	0.36	0.27	0.37	0.59	0.56	0.87	0.70	0.78	0.61	0.50	0.47	0.47	0.53	0.54	0.66	0.64	0.91	0.92
	831	170	75	−203	−237	104	−156	−118	−73	51	115	128	−63	−1	−3	−165	−253	13	−50	36	−19	−118	52	66	−19	9	161
${}_{18}S_4$	27	39	44	35	27	32	32	40	55	53	45	50	39	53	44	27	45	31	43	50	48	43	42	35	47	19	20
	0.98	0.93	0.95	0.93	0.93	0.95	0.79	0.82	0.57	0.57	0.53	0.54	0.76	0.79	0.90	0.81	0.83	0.62	0.63	0.51	0.48	0.45	0.46	0.43	0.44	0.91	0.90
	880	16	8	−154	−91	45	−71	36	−11	113	−29	83	−120	−8	−148	−157	−22	−59	−100	−48	91	−40	74	−48	−30	−147	170
${}_{21}S_6$	112	40	69	69	86	78	60	69	61	61	60	55	86	74	56	39	48	58	46	49	47	47	39	46	40	61	51
	0.76	0.93	0.89	0.87	0.84	0.54	0.72	0.66	0.43	0.38	0.40	0.48	0.65	0.64	0.62	0.56	0.55	0.37	0.26	0.25	0.38	0.22	0.22	0.24	0.21	0.55	0.51
	756	722	−146	−81	−307																						
${}_{22}S_1$	33	118	156	31	40																						
	0.92	0.66	0.63	0.96	0.98																						
	775	200	0	−301	−205	5	2	−116	−159	−74	−209	−107	85	85	173	−25	60	−119	−37	−83	−52	15	28	−137	−40	112	82
${}_{23}S_4$	56	54	64	80	92	58	49	51	60	56	82	80	82	95	44	40	39	49	44	40	58	43	42	44	58	32	28
	0.94	0.87	0.88	0.85	0.84	0.86	0.58	0.61	0.38	0.40	0.39	0.35	0.61	0.58	0.69	0.65	0.70	0.38	0.42	0.27	0.28	0.27	0.21	0.47	0.45	0.91	0.90
	670	13	147	−33	−334	62	−166	−111	−86	80	−33	100	270	244	−5	−37	−249	−14	−94	−68	−96	74	44	−5	9	−26	22
${}_{23}S_5$	36	37	42	35	54	20	35	34	48	47	51	64	60	79	32	−37	47	54	30	22	43	33	30	48	40	46	44
	0.93	0.85	0.87	0.86	0.77	0.83	0.62	0.58	0.33	0.32	0.23	0.30	0.49	0.51	0.67	0.49	0.43	0.19	0.26	0.12	0.21	0.17	0.17	0.12	0.12	0.39	0.50
	557	−228	537	115	131																						
${}_{27}S_1$	106	222	185	103	100																						
	0.87	0.30	0.66	0.95	0.95																						
	826	161	−232	76	−289	281	255	191	−351	96	89	−44	26	−73													
${}_{27}S_2$	82	201	137	122	100	82	264	108	107	90	144	194	58	61													
	0.95	0.88	0.85	0.78	0.78	0.93	0.77	0.86	0.69	0.68	0.69	0.76	0.97	0.93													

Splitting function expanded using the real spherical harmonic convention of Stacey (1977), $\eta(\theta,\phi)=\sum_s\sum_{t=0}^{s}(A_s^t\cos t\phi+B_s^t\sin t\phi)p_s^t(\theta)$. The coefficients are in units of 10^{-6}. The complex coefficients c_{st} are related to the real coefficients by $c_{s0}=1/\sqrt{4\pi}$ and c_{st}, $t>0$, $=(-1)^t\sqrt{2\pi}(A_s^t-iB_s^t)$. The second entry for each mode is the estimated uncertainty of each coefficient determined using a bootstrap approach and the third entry lists the corresponding element of the resolution matrix, with one being perfect resolution.

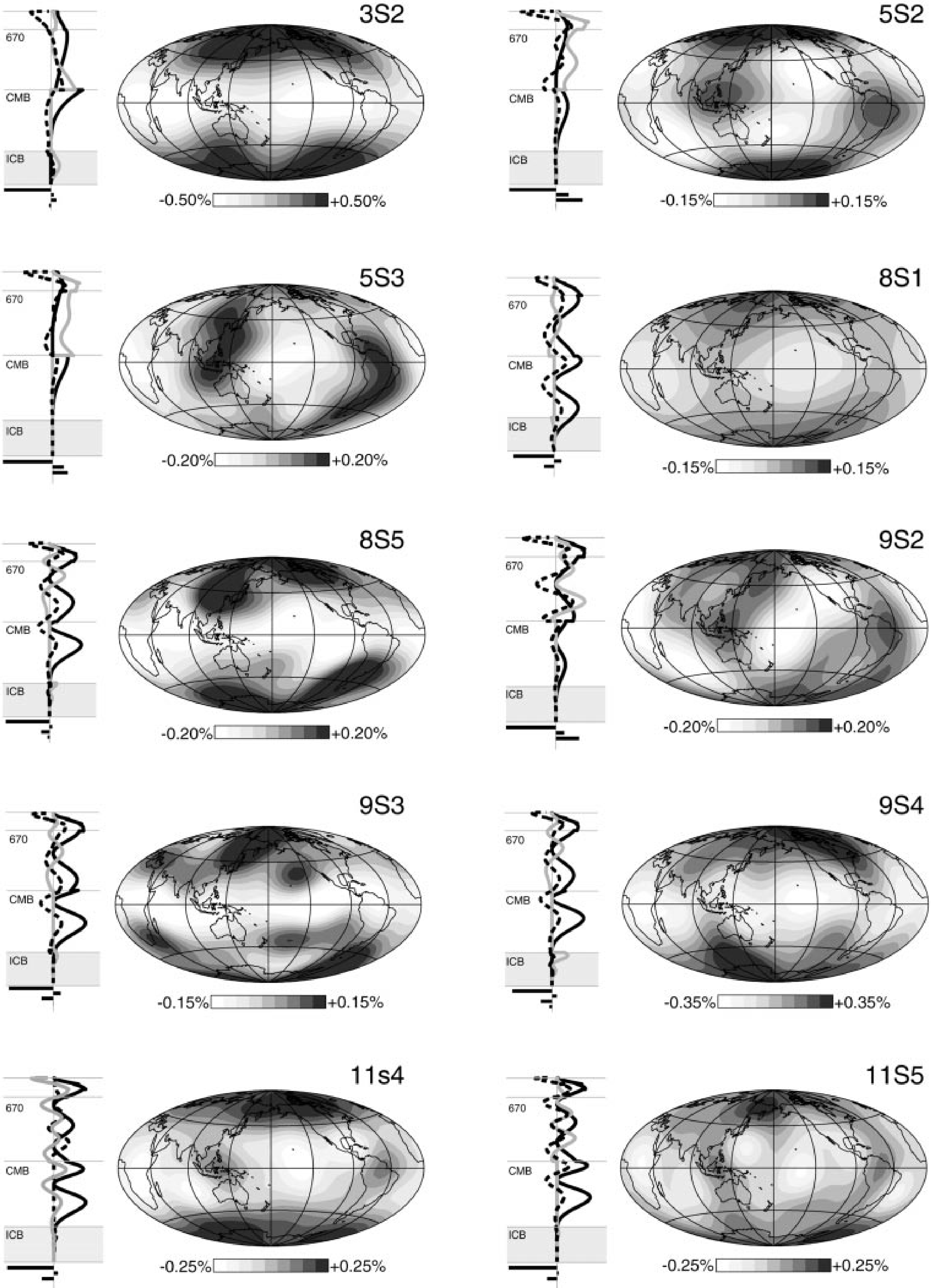

Figure 5. Retrieved splitting functions for 25 inner-core-sensitive normal modes (right) and their sensitivity to radial perturbations in v_p (solid), v_s(grey) and ρ(dashed) (left).

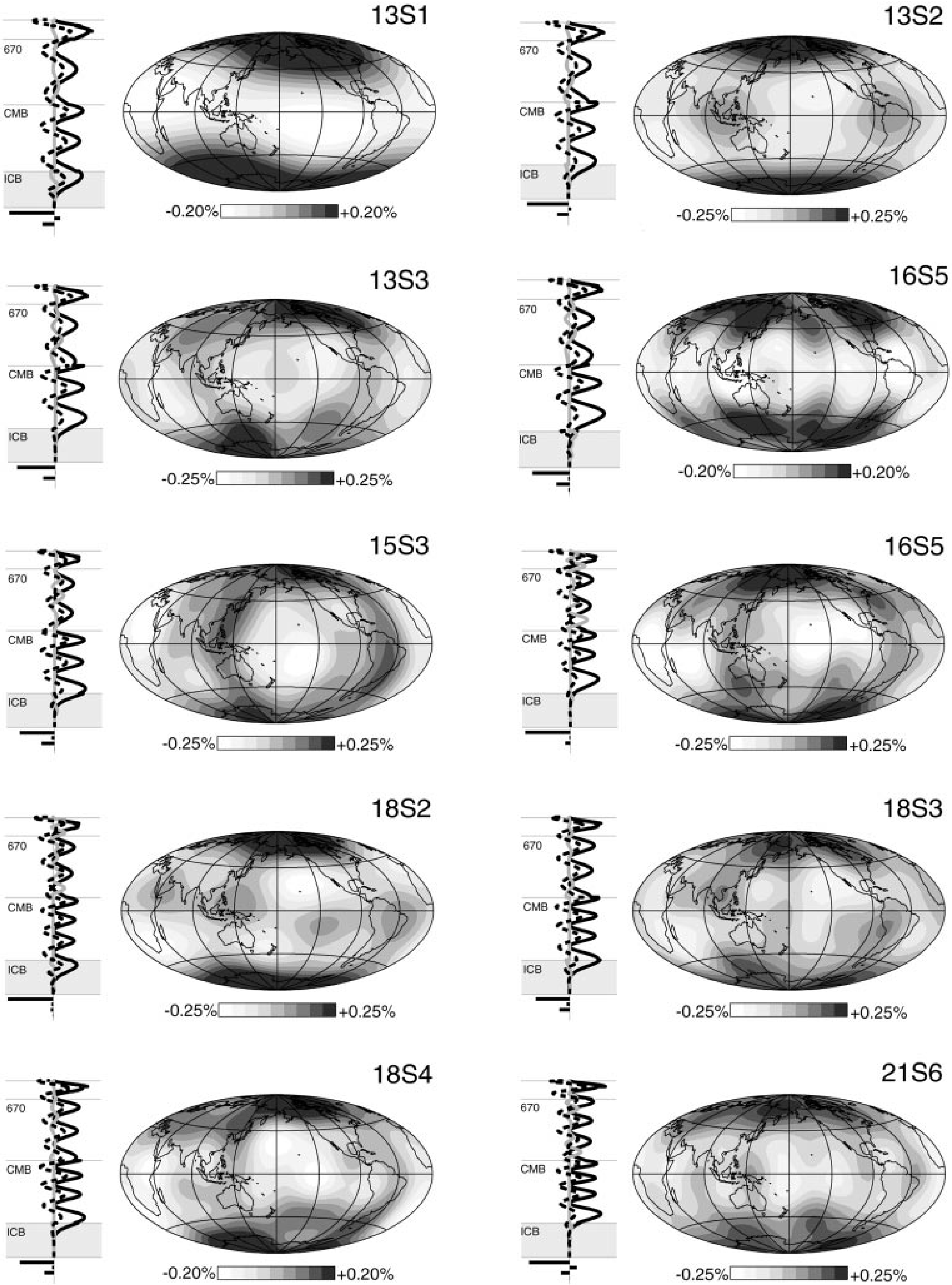

Figure 5. (*Continued.*)

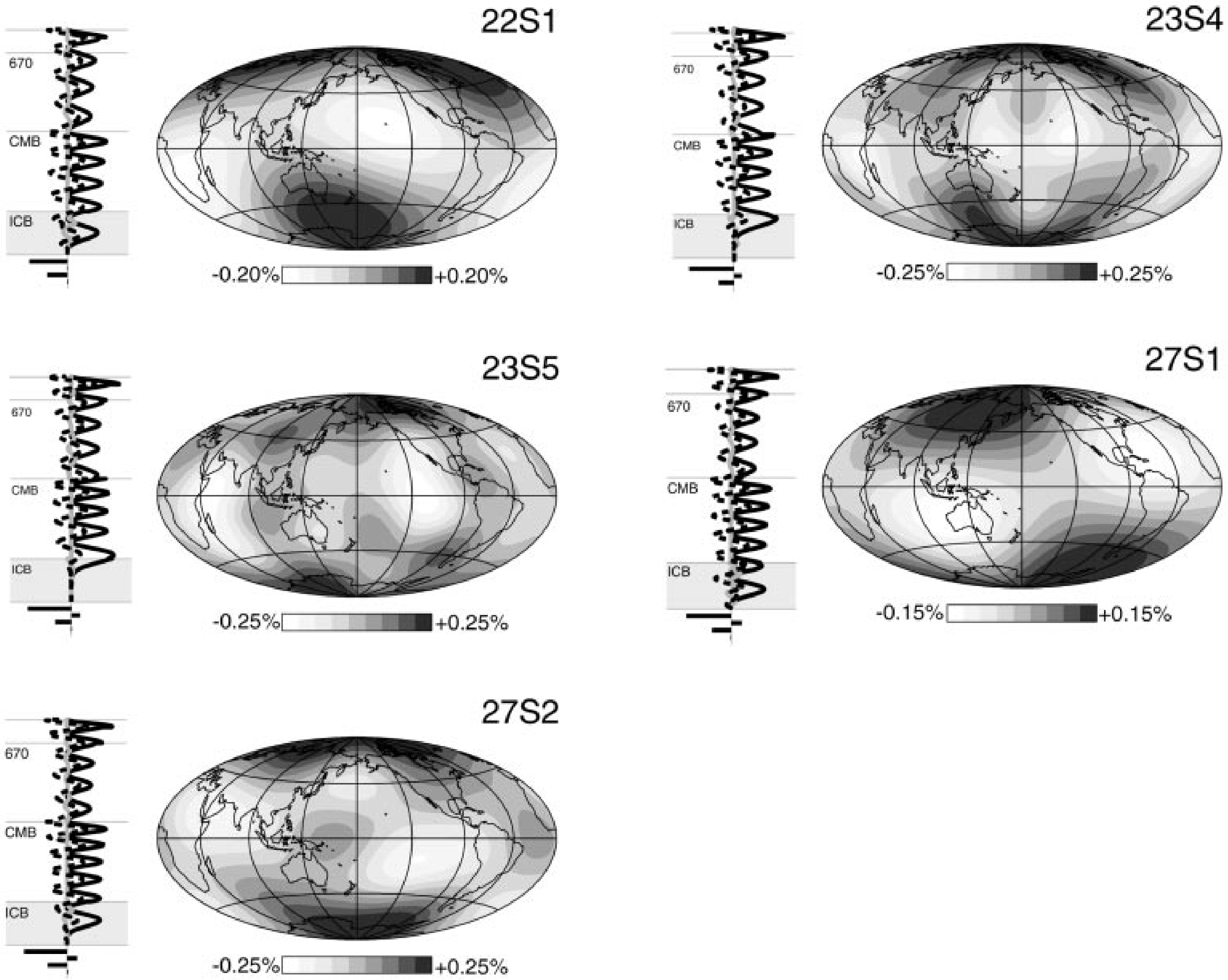

Figure 5. (*Continued.*)

Anisotropic structure

We consider three classes of anisotropic models for the inner core.

Constant cylindrical anisotropy

The initial parametrization considers the simplest departure from isotropy, a cylindrically anisotropic structure with constant strength and fast axis parallel to the rotation axis. Such a structure is characterized by five elastic constants, A, C, F, L and N, where $A=V_{pv}^2\rho$, $C=V_{ph}^2\rho$ describe the anisotropy in P velocity, $L=V_{sv}^2\rho$ and $N=V_{sh}^2\rho$ describe the anisotropy in S velocity, and F is related to the squared velocity at intermediate propagation angles. Transverse isotropy may be completely described by a degree 4 spherical harmonic expansion of the elastic tensor $\Lambda_{s0}^{\alpha\beta\gamma\delta}$ (Tanimoto 1986; Mochizuki 1987; Tromp 1995b). In this case, the 26 coefficients are linear combinations of the five elastic constants.

Radially varying cylindrical anisotropy

In the next case, we allow the strength of the five elastic constants to vary with radius, $A(r)$, $C(r)$, $F(r)$, $L(r)$ and $N(r)$ (e.g. Woodhouse *et al.* 1986; Li *et al.* 1991; Tromp 1995) by parametrizing the radial variability using polynomials of order 4 in radius r. However, only even-order polynomials occur in the description of splitting for an isolated multiplet (Li *et al.* 1991). We are thus left with 15 free parameters to determine.

While there are clear indications that anisotropy is more complicated than radially varying transverse isotropy, this characterization is still common in analyses of traveltime anomalies and is used for calculations of the rate of differential rotation (e.g. Song & Richards 1996; Su *et al.* 1996).

Axisymmetric anisotropy

Following Li *et al.* (1991), we relax the form of allowable anisotropy by removing the requirement of transverse isotropy. To maintain a manageable number of unknowns in the inversion, we restrict the anisotropy to being axisymmetric relative to the rotation axis, consistent with the fact that the dominant signal in the normal mode spectra is due to zonal structures. For lateral structure expanded to degree 4 in spherical harmonics and radial polynomials of orders 2 and 4, there are 38 coefficients that contribute to isolated mode splitting while maintaining the non-singularity of the elastic tensor at the centre of the core.

Although evidence exists for a departure of the symmetry axis from the rotation axis by roughly 10° (Shearer & Toy 1991;

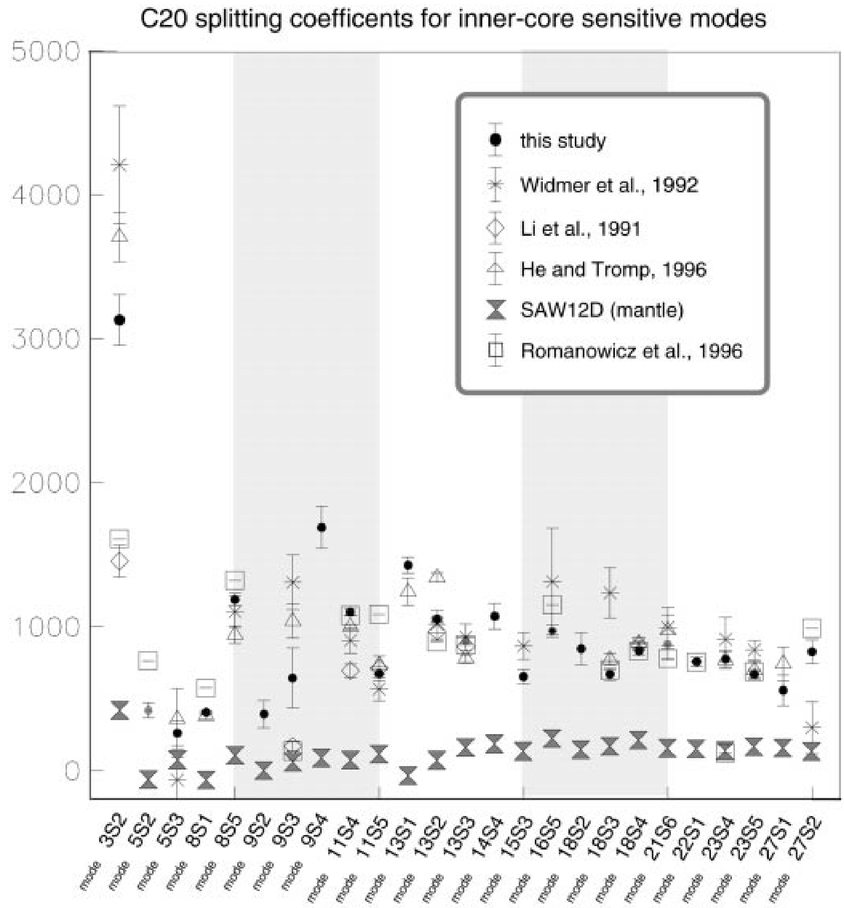

Figure 6. Comparison of the retrieved c_{20} splitting coefficient with published values and the predictions of a current mantle mode (Li & Romanowicz 1996).

Creager 1992; Su & Dziewonski 1995; Romanowicz *et al.* 1996), it is not well resolved in normal mode data and we have not incorporated it into the parametrization.

Isotropic structure

The modes considered are sensitive to isotropic structure throughout Earth, both in the mantle and core.

Inner Core

In the inner core, there is evidence that a portion of the traveltime signal is consistent with isotropic heterogeneity in compressional velocity (e.g. Su & Dziewonski 1995; Tanaka & Hamaguchi 1997). Allowing only anisotropic structure in the inner core assumes that there is no chemical or thermal variability in the core that would give rise to significant isotropic heterogeneity. Since there are indications that the inner core contains isotropic heterogeneity, we include zonal isotropic heterogeneity of lateral degree 4 and radial order 4, adding six additional parameters.

Mantle heterogeneity

We first consider that mantle structure is well described by existing tomographic mantle models, and correct the mode data using the shear velocity model SAW12D (Li & Romanowicz 1996). We only consider the structure through spherical harmonic degree 6, since many mantle models are well correlated at this wavelength (e.g. Laske & Masters 1995). In later discussion, we will examine the effect of using different mantle models on the inferred inner core structure.

Reference model: correction to centre frequency

When modelling the splitting of normal modes, a failure to align the predicted and observed spectra leads to incorrect modelling and poor fitting of the spectra. To allow for optimal alignment of the modes, we parametrize perturbations to the radial isotropic velocity structure in the mantle ($V_P(r)$, $V_S(r)$), using order 4 Chebyshev polynomials. We perturb $V_P(r)$ in the inner core using polynomials of order 2.

Inversion procedure

Normal modes

The spectral observations of a single mode observed following several events are weighted as discussed previously. In the combined inversion of all modes, the individual modes are weighted to provide equal contributions to the final model. We exclude the modes ${}_9S_3$, ${}_{14}S_4$, ${}_{27}S_2$, ${}_{27}S_1$ and ${}_{21}S_6$ due to the poor convergence behaviour of these modes in the non-linear

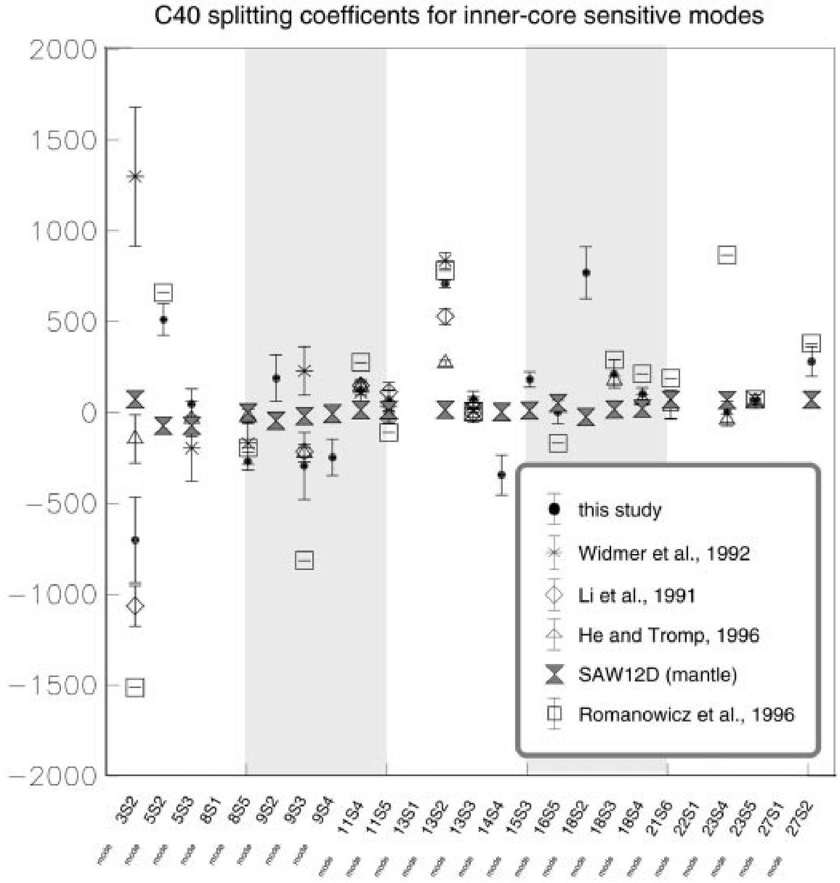

Figure 7. Comparison of the retrieved c_{40} splitting coefficient with published values and the predictions of a current mantle mode (Li & Romanowicz 1996).

estimation of the splitting functions, but we will examine the consistency of the final model with these modes.

Traveltime data

Since normal modes lack sensitivity to the centre of the inner core, we incorporate a subset of deep-turning *PKP* differential traveltime observations (Souriau & Romanowicz 1996; Vinnik *et al.* 1994; Song 1996). The traveltimes are upweighted to provide a quarter of the total data variance, to ensure their contribution to the final model.

Starting solution

While the retrieval of individual splitting functions is strongly dependent on the starting model chosen, the direct inversion commonly converges starting from a spherical reference model. Adequate convergence requires 5–6 iterations. We find that the convergence is enhanced if, after the first three iterations, the perturbations to the radial reference model are zeroed before additional iterations.

RETRIEVED MODELS

For this initial set of inversions, Table 6 provides the variance reduction to the individual mode spectra and traveltime data while Table 7 lists the fits to the splitting coefficients retrieved in the previous section.

Table 6. Residual variance for different parametrizations of inner core anisotropy.

Mode	Inner core parametrization		
	Transverse isotropy		
	Constant	Radial	Axisymmetric
$_3S_2$	0.33	0.36	0.31
$_5S_2$	0.40	0.41	0.37
$_5S_3$	0.20	0.20	0.19
$_8S_1$	0.31	0.30	0.29
$_8S_5$	0.43	0.43	0.43
$_9S_2$	0.64	0.63	0.63
$_9S_4$	0.40	0.39	0.37
$_{11}S_4$	0.66	0.40	0.35
$_{11}S_5$	0.36	0.31	0.27
$_{13}S_1$	0.34	0.64	0.42
$_{13}S_2$	0.48	0.44	0.35
$_{13}S_3$	0.42	0.39	0.41
$_{15}S_3$	0.92	0.85	0.73
$_{16}S_5$	1.28	1.24	0.95
$_{18}S_2$	2.74	0.84	0.51
$_{18}S_3$	1.13	0.70	0.73
$_{18}S_4$	0.44	0.54	0.53
$_{22}S_1$	0.97	0.59	0.61
$_{23}S_4$	0.68	0.61	0.62
$_{23}S_5$	1.38	0.77	0.73
Total	0.73	0.55	0.48
Traveltimes	0.24	0.22	0.14

Table 7. Summary of inversions for inner core anisotropy.

Mantle (fixed)	Model Parameterization: Isotropic	Model Parameterization: Inner Core	Residual Variance: Mode Spectra	Residual Variance: Travel Times	Splitting Coefficients† C00	Splitting Coefficients† C20	Splitting Coefficients† C40
SAW12D	mantle: dVs(r),dVp(r) inner core: dVp(r)	Transverse Isotropy: constant	**0.73**	**0.24**	**0.62**	**0.24**	**2.23**
		Transverse Isotropy: radial	**0.55**	**0.22**	**0.39**	**0.36**	**2.53**
		Axisymmetric	**0.48**	**0.14**	**0.39**	**0.25**	**0.90**
SAW12D	correction to dC00 for each mode	Transverse Isotropy: constant	**0.62**	**0.48**	**0.42**	**0.14**	**1.03**
		Transverse Isotropy: radial	**0.52**	**0.26**	**0.27**	**0.19**	**1.00**
		Axisymmetric	**0.46**	**0.21**	**0.28**	**0.17**	**0.68**
S4W4.m10*	mantle: dVs(r),dVp(r) inner core: dVp(r)	Axisymmetric	**0.52**	**0.14**	**0.40**	**0.19**	**0.57**

* S4W4.m10 was derived independently from 10 isolated mantle-sensitive normal modes

† splitting coefficients not used as data in inversion

Constant transverse isotropy

For constant anisotropy with the symmetry axis parallel to the rotation axis, we retrieve the following combinations of the five elastic parameters that are resolved:

(1) the fractional difference in velocity for equatorial and axial travelling P waves (compressional anisotropy),

$$\epsilon=\frac{1}{2}(A-C)/A_0=2.5 \text{ per cent}, \tag{16}$$

where A_0 is the reference velocity;

(2) the fractional difference in velocity for equatorial and axial travelling S waves (shear anisotropy),

$$\sigma=\frac{1}{2}(N-L)/N_0=0.4 \text{ per cent}, \tag{17}$$

$$\gamma=\frac{-1}{4}(1/2A+1/2C-2L-F)/A_0=0.1 \text{ per cent}. \tag{18}$$

The value of ϵ of 2.5 per cent is reasonably close to that obtained by body wave studies; Su & Dziewonski (1995) and Tromp (1995a) found peak levels of P-wave anisotropy not exceeding 3 per cent, while other studies argued for an average level of 3–3.5 per cent. The value of γ governing anisotropy for meridionally polarized S waves (S_{med}) is smaller than that predicted theoretically (~ 10 per cent) by Stixrude & Cohen (1995) or inferred by body wave analyses (e.g. Su & Dziewonski 1995) but is similar to that inferred by Tromp (1995a). The value of σ that describes anisotropy for equatorially polarized S waves (S_{eq}) is in better agreement with the theoretical value. If traveltimes are not included in the inversion, the P-wave anisotropy drops to 1.8 per cent, which we attribute to the limited resolution achievable using only normal mode data.

From the values in Table 6, column 1, and Table 7, row 1, this simple model of anisotropy can simultaneously explain an appreciable level of variance in the c_{20} splitting coefficient (75 per cent) as well as the traveltimes (76 per cent). The consistency of the degree 2 splitting coefficient is not unexpected, given the linear trend between the retrieved coefficients and the rms kernels for this simple structure (Fig. 8). Upon closer inspection, however, it is clear that a subset of the normal mode spectra remains unexplained by this simplified structure, especially ${}_{18}S_2$, ${}_{16}S_5$, ${}_{18}S_3$, ${}_{22}S_1$ and ${}_{23}S_5$. In addition, the degree 4 splitting coefficients are poorly estimated by this model, suggesting the necessity of additional complexity (Romanowicz *et al.* 1996).

Radially varying transverse isotropy

When variability in the radial strength of anisotropy is introduced (Fig. 9), a minimum in P-wave anisotropy appears around 300 km below the ICB, similar in character to that observed using traveltimes (Su & Dziewonski 1995) and normal modes (Tromp 1995a). Near the surface, the level of anisotropy is roughly 3 per cent, consistent with previous body wave studies. The anisotropy peaks at 5 per cent in the centre of the core, again similar in character to the body wave model of Su & Dziewonski (1995). The S-wave anisotropy deviates by less than 2 per cent at all depths.

The added flexibility has significantly improved the fit to several individual modes and reduced the total misfit to the mode spectra from 0.73 to 0.55. However, the fit to the traveltimes has not been reduced significantly and the predicted c_{40} splitting coefficients (Table 8, row 2) remain strongly discrepant (interestingly, the ability to explain the degree 2 coefficients has also degraded). It is thus clear that there are signals in the data that cannot be modelled with cylindrical anisotropy.

Axisymmetric expansion of the general elastic tensor

Since the inversions with cylindrical anisotropy are unable to explain all aspects of the data, in this section we consider a more general expansion of the anisotropic elastic tensor under the restriction that the structure remain axisymmetric (Li *et al.* 1991; Romanowicz *et al.* 1996).

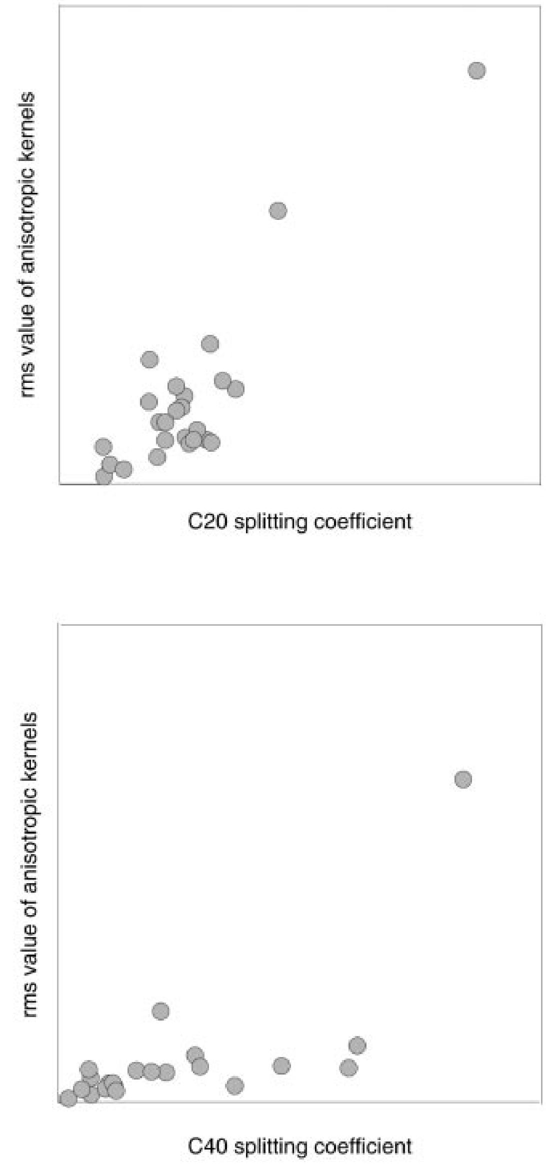

Figure 8. The residual splitting coefficients c_{20} (top) and c_{40} (bottom) compared to the rms of the anisotropic kernels in the inner core, under the restrictive assumption of transverse isotropy with symmetry axis aligned with the rotation axis. The coefficients represent the residual signal after the predictions for ellipticity, rotation and mantle model SAW12D (Li & Romanowicz 1996) have been removed.

Fig. 10 presents a cross-section through the inner core with P-wave velocity variations for waves *travelling parallel to the rotation axis*, showing velocities up to 4.5 per cent faster than average. The region of fast velocity concentrated near the centre of the core for the radially varying transversely isotropic models is now elongated in the direction of the rotation axis (if the data were satisfied by a model of cylindrical anisotropy, the contours would be concentric circles). This structure is consistent with the results of Romanowicz *et al.* (1996), who applied a two-step inversion to a smaller data set. The retrieved isotropic heterogeneity is relatively insignificant, with variations in structure of less than 1 per cent.

For polar-parallel propagating P waves, the optimal model of anisotropy also predicts a shallow region of increased

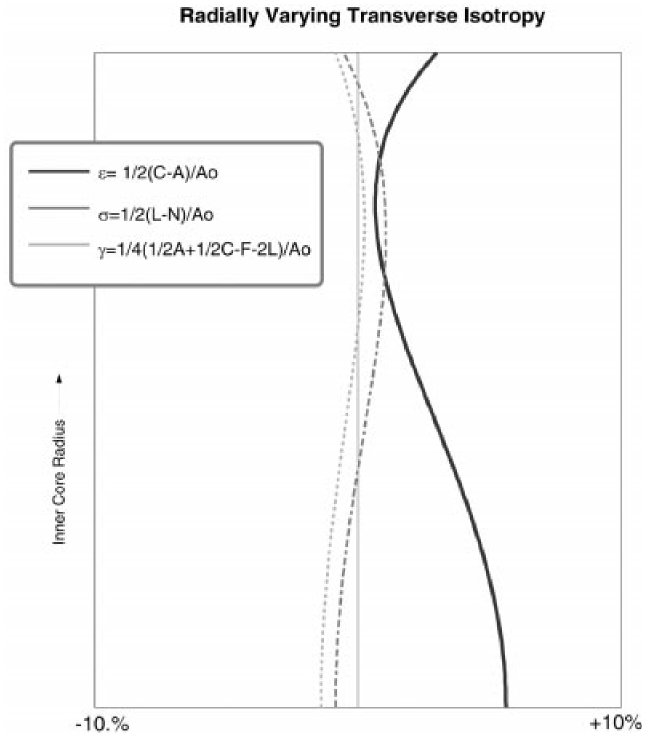

Figure 9. Radial variability of P-wave anisotropy (ϵ) and S-wave anisotropy (σ, γ) in per cent.

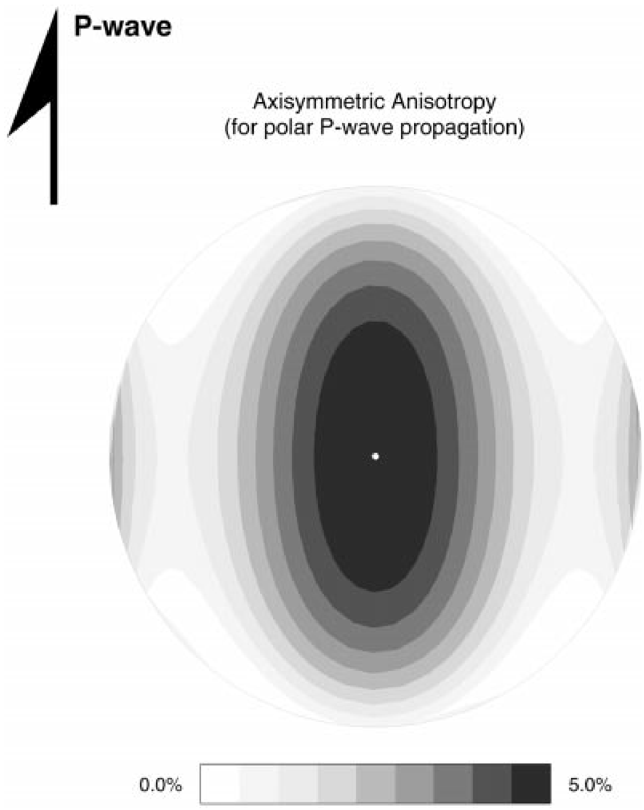

Figure 10. Cross-section through the inner core for an axisymmetric model showing velocity perturbations for P waves *travelling parallel to the rotation axis*.

Table 8. Residual variance of modes for a shallow isotropic layer.

Mode	Thickness of isotropic layer (km)			
	0	100	200	300
${}_3S_2$	0.36	0.36	0.38	0.42
${}_5S_2$	0.41	0.43	0.43	0.38
${}_5S_3$	0.20	0.20	0.20	0.20
${}_8S_1$	0.30	0.29	0.29	0.30
${}_8S_5$	0.43	0.45	0.46	0.47
${}_9S_2$	0.63	0.63	0.63	0.64
${}_9S_4$	0.39	0.47	0.70	0.94
${}_{11}S_4$	0.40	0.36	0.41	0.59
${}_{11}S_5$	0.31	0.32	0.36	0.45
${}_{13}S_1$	0.64	0.57	0.47	0.52
${}_{13}S_2$	0.44	0.41	0.36	0.34
${}_{13}S_3$	0.39	0.39	0.41	0.50
${}_{15}S_3$	0.85	0.89	0.90	0.95
${}_{16}S_5$	1.24	1.24	1.21	1.17
${}_{18}S_2$	0.84	1.06	1.11	0.84
${}_{18}S_3$	0.70	0.81	0.90	1.00
${}_{18}S_4$	0.54	0.56	0.56	0.58
${}_{22}S_1$	0.59	0.60	0.59	1.06
${}_{23}S_4$	0.61	0.59	0.58	0.58
${}_{23}S_5$	0.77	0.86	0.92	1.07
Total	0.55	0.57	0.59	0.65

axis-parallel velocity, which if robust would also be expected if alignment due to general convection was the dominant mechanism of anisotropy (Romanowicz *et al.* 1996). The predicted traveltime anomaly of almost 2 s for waves bottoming at 100 km is larger than that observed from body wave studies by a factor of two (e.g. Su & Dziewonski 1995), but the predicted anomaly decreases to roughly 0.5 s when the propagation direction is tilted 20° relative to the rotation axis.

The departure from radial symmetry increases the compatibility of the spectral observations and the traveltime data with clear reductions in residual variances (Table 6, column 3). In addition, the predicted splitting coefficients are in better agreement with those retrieved in the previous section (Table 7, row 3), especially for the degree 4 terms (the residual variance dropping from 2.5 to 0.9).

Fig. 11 presents the perturbation in the radial isotropic compressional and shear velocities; in all cases, these are less than 0.5 per cent. While we do not consider these perturbations to be well enough resolved to provide reliable corrections to the reference model, we note that the character of the perturbations is similar for all inversions described above. Interestingly, the isotropic velocity at the top of the inner core is reduced slightly, consistent with the inferences of Song & Helmberger (1992).

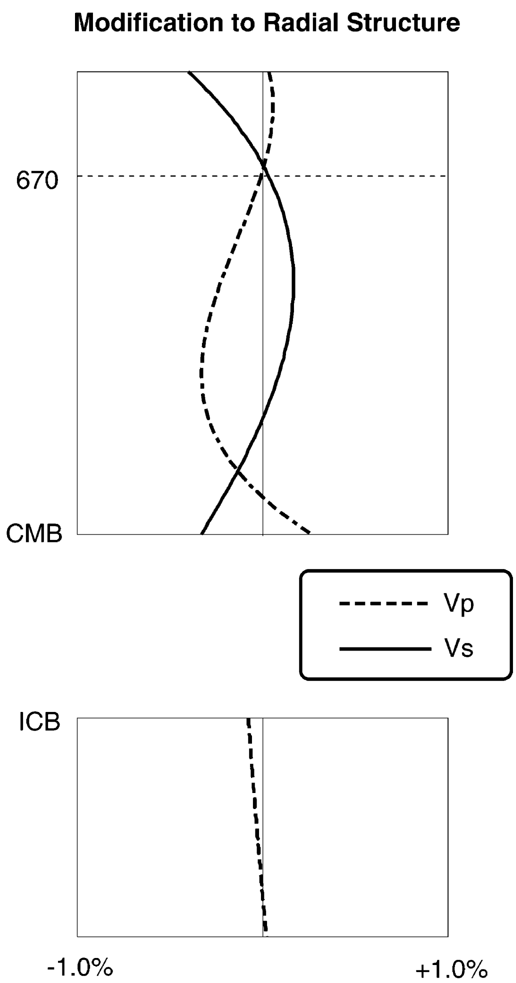

Figure 11. Perturbations to (top) radial compressional and shear velocity in the mantle and (bottom) radial compressional velocity in the inner core.

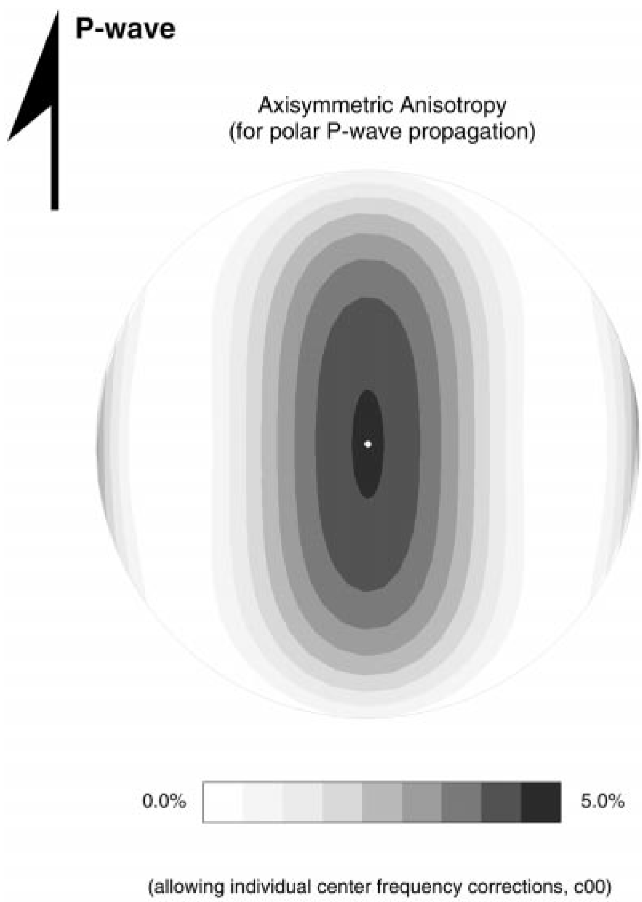

Figure 12. Cross-section through the inner core for an axisymmetric model showing velocity perturbations for *P* waves *travelling parallel to the rotation axis* retrieved when perturbations to each mode centre frequency are introduced into the inversion.

EFFECTS OF ISOTROPIC RADIAL STRUCTURE AND MANTLE HETEROGENEITY

While consideration of general axisymmetric anisotropy is better able to explain the observations than transversely isotropic structure, the misfit to the anomalous c_{40} coefficients remains high (residual variance of 0.90; Table 7, row 3). In contrast, a linear inversion of splitting coefficients for inner core anisotropy is able to explain more than 50 per cent of the variance in the c_{40} splitting coefficients (Romanowicz *et al.* 1996). To examine this apparent discrepancy and investigate potential trade-offs with isotropic structure, we (1) perform a direct inversion with greater flexibility in modelling the mode centre frequencies, and (2) examine the effect of the (fixed) mantle structure.

To align the centre frequencies better in the first experiment, we replace the parametrization for radial isotropic velocity perturbations (which acts only to modify the centre frequencies) with an explicit correction to the centre frequency for each mode. The inversion has complete freedom to determine the best centre frequency for each mode, with no requirement that they be consistent with any radial model of structure. The retrieved inner core models are not significantly different (e.g. Fig. 12) and the fit to the spectra (Table 7, rows 4–6) improves slightly for each of the three parametrizations, as expected given the additional degrees of freedom. The fit to the travel-times has degraded slightly, suggesting that some of the inner core signal in the normal modes is being absorbed into the centre frequency corrections, δc_{00}. The prominent difference from the previous inversions is that the fit to all splitting coefficients is uniformly improved at the level of 50 per cent. We interpret this as indicating a trade-off between fitting the centre frequency and explaining the splitting of the mode, a trade-off that does not significantly impact the inferred inner core structure (as seen by comparing Figs 12 and 10). From the result of this experiment, we conclude that the parametrization of radial isotropic structure, in conjunction with the fixed mantle model, is too restrictive to model the anomalous isotropic signal in the data completely.

We are reluctant simply to increase the number of degrees of freedom in the radial isotropic parametrization since experiments suggest that this leads to large radial velocity perturbations. Instead, we examine the impact of the chosen mantle model. Our motivation is that each mantle model is published with a relatively short-wavelength degree 0 component, a correction to the radial structure. While most studies do not attach great significance to this radial perturbation, it nonetheless represents the starting model for our perturbation to the radial isotropic structure. Because we are using long-wavelength radial polynomials, small-wavelength radial structure in the starting mantle model cannot be modified even if required by the data.

A significant improvement in explaining the splitting coefficients is obtained when we consider a mantle model based on a limited number of mantle-sensitive modes. We

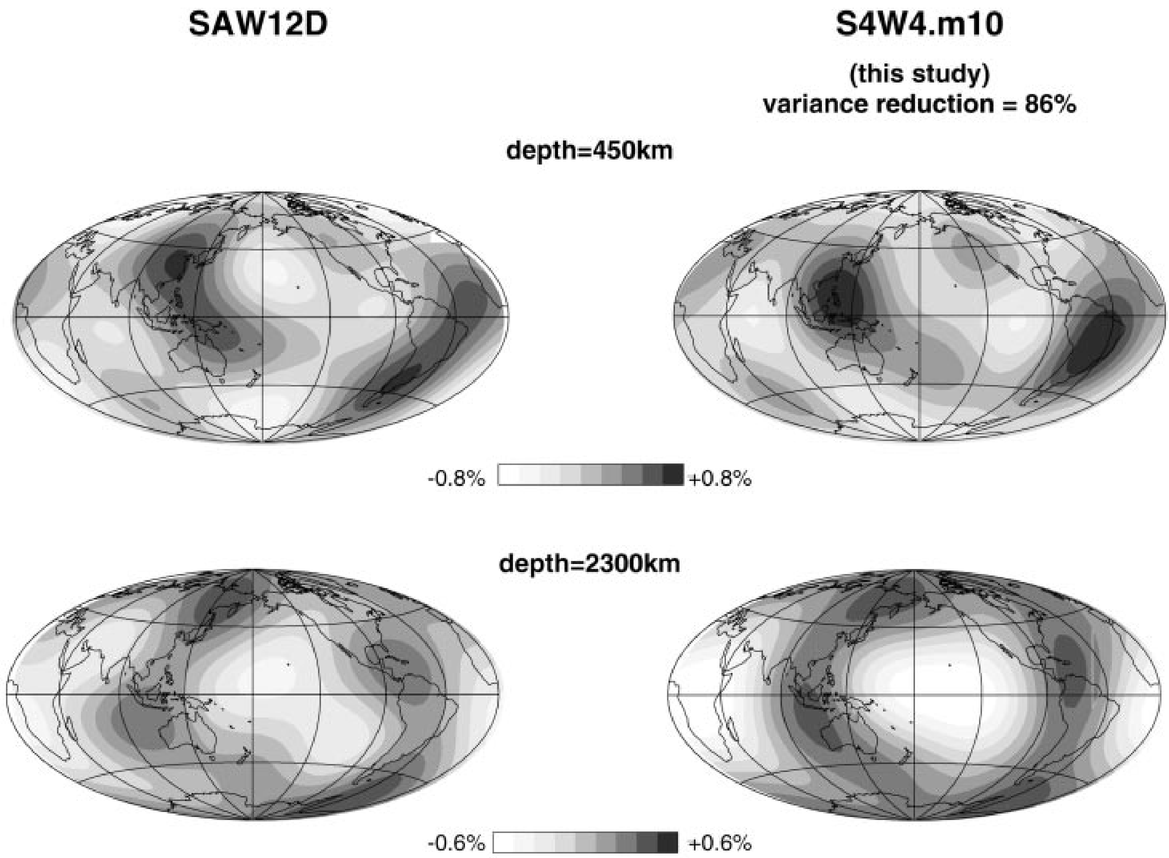

Figure 13. Even-degree 4 mantle model S4W4.m10 (right) based on the direct inversion of 10 mantle-sensitive normal modes compared with SAW12D (Li & Romanowicz 1996) filtered to the same components (left).

have used data for 10 mantle-sensitive-only modes in a direct inversion for degree 4 lateral and order 4 radial mantle shear velocity perturbations (e.g. Li *et al.* 1991; Kuo *et al.* 1997). In the inversion, the density and compressional velocity are assumed to be correlated and proportional to the shear velocity ($d\ln\beta/d\ln\alpha=2.0$, $d\ln\beta/d\ln\rho=4.0$). The resulting model (Fig. 13) has similarities to SAW12D filtered to the same degree, although differences may simply be a consequence of the assumed proportionality constants and the limited data set used in its construction.

We incorporate this mantle model into the direct inversion of inner-core-sensitive modes (the lateral mantle structure is fixed; the degree 0 structure provides a starting model for perturbations to the radial structure). The resulting inner core anisotropic structure (Fig. 14) has not changed significantly. However, the resulting models are better able to explain the splitting coefficients (Table 7, row 7) with a residual variance of 0.57 for the c_{40} terms. The fit to the traveltimes is maintained while the fit to the spectra is decreased slightly due almost completely to a difficulty in fitting ${}_{22}S_1$. We do not claim that we have developed an improved model of the mantle; the data applied to the problem are too few. Rather, we stress that our mantle model, when combined with the axisymmetric parametrization of inner core anisotropy, is more consistent with the specific and limited set of inner-core-sensitive spectra considered in this study. We also note that this mantle model is most consistent with the spectra under the restriction that we allow only perturbations to the zonal (c_{20}, c_{40}) splitting coefficients of each mode.

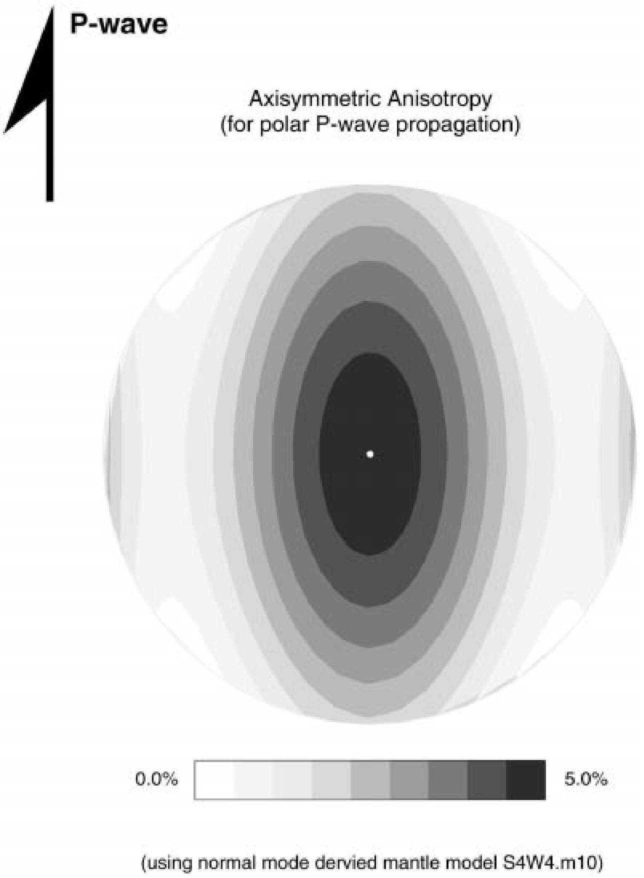

Figure 14. Cross-section through the inner core for an axisymmetric model showing velocity perturbations for *P* waves *travelling parallel to the rotation axis* using mantle model S4W4.m10 as the fixed mantle structure.

For our preferred model, we compare the predicted splitting functions with those retrieved from spectral data as described in the previous section (Fig. 15). For the majority of modes, the predicted and observed splitting functions are remarkably similar in strength and character, including those for modes ${}_{27}S_1$ and ${}_{27}S_2$, which were not used in the one-step inversion for inner core anisotropy. For the shallow-sampling modes ${}_{11}S_4$ and ${}_{11}S_5$, the predictions reproduce the slightly stronger splitting function observed for ${}_{11}S_4$. The only gross difference is an underprediction of the splitting of ${}_{13}S_1$. This difference may indicate non-uniqueness of the retrieved splitting function, a reasonable hypothesis given the strong sensitivity of the $l=1$ modes to the chosen starting model.

Recent analyses of shallow-turning *PKIKP* waves suggest that an isotropic layer may exist in the outer 300 km of the inner core (e.g. Song & Helmberger 1998), which may have implications for mechanisms of core solidification or relaxation times in the shallow outer core (e.g. Buffett 1997). To investigate this hypothesis using the normal mode constraints, we consider inversions for radially varying transverse isotropy in which we impose a shallow isotropic layer of variable thickness. We find, in Table 8, that the fits to several normal modes degrade when the thickness of the isotropic layer exceeds 200 km, with the residual variance for the shallow-sampling modes ${}_{11}S_4$ and ${}_{11}S_5$ increasing by roughly 50 per cent. Interestingly, both shallow-sampling modes (${}_{11}S_4$, ${}_{11}S_5$) and deeper-sampling modes (${}_3S_2$, ${}_{22}S_1$) show degraded fits, leading us to speculate that the unsuccessful attempts to adjust the anisotropy to explain shallow-sampling modes cannot be compensated at depth to maintain the fit to the deeper-sampling modes.

The inner-core-sensitive modes investigated here may be combined with mantle modes for a joint inversion of the whole Earth structure (e.g. Li *et al.* 1991). We would expect ever greater agreement with the spectral data, since the current direct inversion is effectively only perturbing three splitting coefficients per mode. However, preliminary investigations with our limited data set of mantle modes suggest that the strong anomalous degree 2 signal can dominate the inversion, placing unreasonable zonal structure in the mantle to explain the inner-core-sensitive modes better at the expense of the mantle modes. The acquisition of additional mantle-sensitive mode data (Kuo *et al.* 1997) will better constrain the joint inversion of mode spectra for mantle and core structure.

CONCLUSIONS

We have explored a number of improvements in the inversion of normal mode spectra for anisotropic structure in the inner core. The direct ('one-step') inversion allows us to avoid the non-uniqueness problems inherent in the non-linear estimation of normal mode splitting functions. Better fits to the data can be achieved by allowing adjustments in the mode central frequencies and by using a mode-derived mantle model to correct for 3-D mantle structure. By allowing axisymmetric departures from simple transversely isotropic models of anisotropy, we

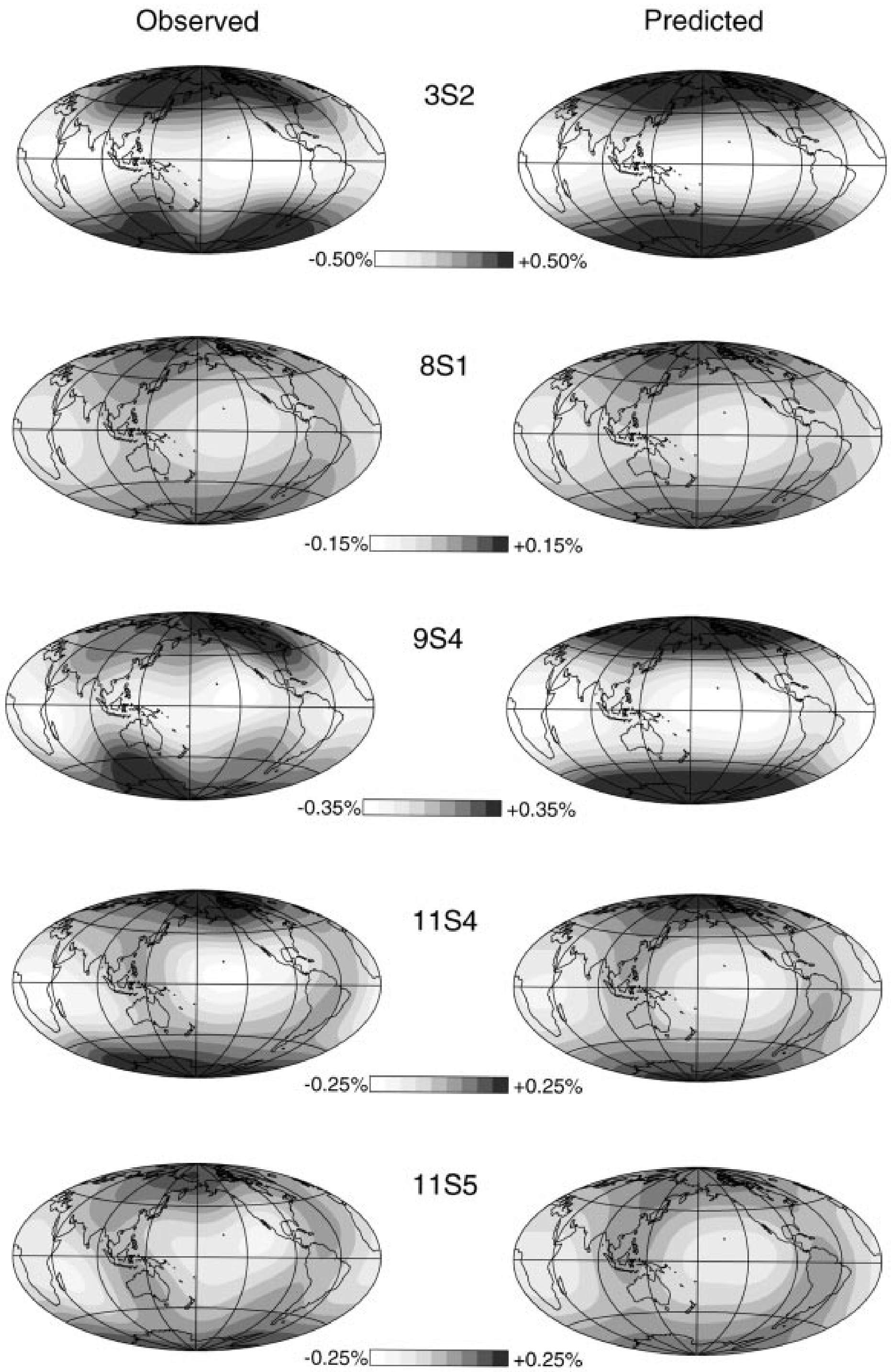

Figure 15. Comparison of observed (left) and predicted (right) splitting functions for the preferred model of inner core anisotropy (Fig. 14) and mantle model S4W4.m10.

confirm the results of Romanowicz *et al.* (1996), namely that improved fits to the data can be obtained with inner core models that have a central zone, elongated in the direction of the rotation axis, with about 3 per cent of anisotropy in *P* velocity, while anisotropy is minimum at mid-depths in the inner core. It is clear that additional complexity beyond axisymmetry exists in the inner core, as illustrated by several recent *PKP* traveltime studies (eg. Tanaka & Hamaguchi 1997; Creager 1997). A more general parametrization of inner core anisotropy, allowing for longitudinal variations, is the subject of current work in our laboratory. Finally, we have verified that an isotropic layer at the top of the inner core, as proposed by Song & Helmberger (1998), degrades the fit to mode splitting data for thicknesses greater than 100–200 km. It is still possible that the shallow inner core structure might be locally isotropic, which would not be resolved by globally sampling modes.

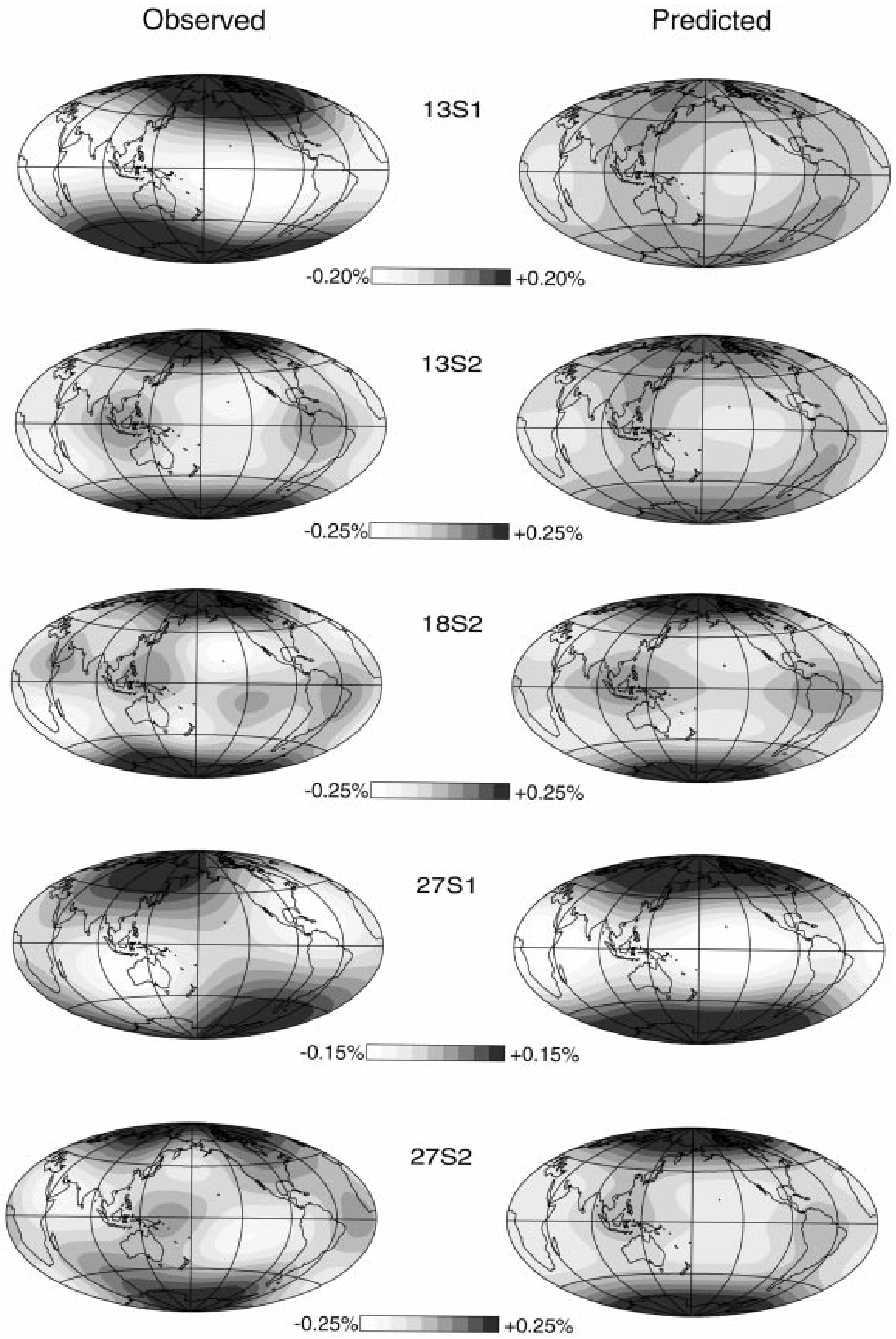

Figure 15. (*Continued.*)

This indicates that there remain yet unresolved discrepancies between normal mode and traveltime data regarding inner core anisotropy. In particular, the strong zonal degree 2 structure inferred by core-sensitive modes is incompatible with the dominance of shallow degree 1 structure in inner core anisotropy documented by Tanaka & Hamaguchi (1997). The present study was conducted under the assumption that all of the anomalous splitting originates within the inner core, based on a consensus reached over the past decade after a long debate in which other possible explanations such as outer core structure have been proposed as alternatives (e.g. Widmer *et al.* 1992). However, the hypothesis of contributions of isotropic structure to anomalous observations may need revisiting in light of studies suggesting an isotropic layer at the top of the inner core as well as the results of Breger & Romanowicz (1998), which indicate that much of the anomalous signal present in deep-core-penetrating *PKP* waves can be explained by structure within D″.

ACKNOWLEDGMENTS

We appreciate the detailed reviews and helpful suggestions of Jeroen Tromp and Ruedi Widmer. Discussions with Guy Masters, Adam Dziewonski, Xi Song and Don Helmberger helped to improve the study. This work was partially supported under a National Science Foundation Postdoctoral Fellowship. This study is contribution 99-03 of the Berkeley Seismological Laboratory.

REFERENCES

Breger, L.L. & Romanowicz, B., 1998. Evidence for strong lateral heterogeneity near the core-mantle boundary in the central Pacific, *EOS, Trans. Am. geophys. Un.,* **79,** F608 (abstract).

Buffett, B.A., 1997. Geodynamic estimates of the viscosity of the Earth's inner core, *Nature,* **388,** 571–573.

Creager, K.C., 1992. Anisotropy in the inner core from differential travel times of the phases PKP and PKIKP, *Nature,* **356,** 309–314.

Creager, K.C., 1997. Three-dimensional anisotropic structure and rotation of the inner core, *EOS, Trans. Am. geophys. Un.,* **78,** 458.

Dahlen, F.A., 1968. The normal modes of a rotating, elliptical earth, *Geophys J. R. astr. Soc.,* **16,** 329–367.

Dahlen, F.A., 1969. The normal modes of a rotating, elliptical earth, II, Near resonant multiplet coupling, *Geophys. J. R. astr. Soc.,* **18,** 397–436.

Dahlen, F.A., 1982. The effect of data windows on the estimation of free oscillation parameters, *Geophys. J. R. astr. Soc.,* **69,** 537–549.

Dziewonski, A.M. & Anderson, D.L., 1981. Preliminary reference Earth model (PREM), *Phys. Earth planet. Inter.,* **25,** 297–356.

Dziewonski, A.M., Chou, T.-A. & Woodhouse, J.H., 1981. Determination of earthquake source parameters from waveform data for studies of global and regional seismicity, *J. geophys. Res.,* **86,** 2825–2852.

Giardini, D., Li, X.-D. & Woodhouse, J.H., 1988. Splitting functions of long-period normal modes of the Earth, *J. geophys. Res.,* **93,** 13 716–13 742.

Gilbert, F. & Dziewonski, A.M., 1975. An application of normal mode theory to the retrieval of structural parameters and source mechanisms from seismic spectra, *Phil. Trans. R. Soc. Lond.,* A**278,** 189–269.

He, X. & Tromp, J., 1996. Normal-mode constraints on the structure of the Earth, *J. geophys. Res.,* **101,** 20 053–20 082.

Kuo, C., Durek, J. & Romanowicz, B., 1997. Direct inversion of normal mode spectra for mantle heterogeneity, *EOS, Trans. Am. geophys. Un.,* **78,** F460 (abstract).

Laske, G. & Masters, G., 1995. Frequency-dependent polarization measurements of long-period surface waves and their implications for global phase-velocity maps, *Phys. Earth planet. Inter.,* **84,** 111–137.

Li, X.-D. & Romanowicz, B., 1996. Global mantle shear velocity model developed using nonlinear asymptotic coupling theory, *J. geophys. Res.,* **101,** 22 245–22 272.

Li, X.-D., Giardini, D. & Woodhouse, J.H., 1991. Large-scale three-dimensional even-degree structure of the Earth from splitting of long-period normal modes, *J. geophys. Res.,* **96,** 551–577.

Masters, G. & Gilbert, F., 1981. Structure of the inner core inferred from observations of its spheroidal shear modes, *Geophys. Res. Lett.,* **8,** 569–571.

Megnin, C. & Romanowicz, B., 1995. Estimation of inner core mode splitting functions combining a genetic algorithm with a direct iterative inversion scheme, *EOS, Trans. Am. geophys. Un.,* **76,** 355 (abstract).

Mochizuki, E., 1987. Application of group theory to free oscillations of an anisotropic rectangular parallelepiped, *J. Phys. Earth,* **35,** 159–170.

Morelli, A., Dziewonski, A.M. & Woodhouse, J.H., 1986. Anisotropy of the inner core inferred from PKIKP travel times, *Geophys. Res. Lett.,* **13,** 1545–1548.

Phinney, R.A. & Burridge, R., 1973. Representation of the elastic-gravitational excitation of a spherical earth model by generalized spherical harmonics, *Geophys. J. R. astr. Soc.,* **34,** 451–487.

Poupinet, G., Pillet, R. & Souriau, A., 1983. Possible heterogeneity of the earth's core deduced from PKIKP travel times, *Nature,* **305,** 204–206.

Resovsky, J.S. & Ritzwoller, M.H., 1995. Constraining odd-degree Earth structure with coupled normal modes, *Geophys. Res. Lett.,* **22,** 2301–2304.

Resovsky, J.S. & Ritzwoller, M.H., 1998. New and refined constraints on three-dimensional Earth structure from normal modes below 3 mHz, *J. geophys. Res.,* **103,** 783–810.

Ritzwoller, M., Masters, G. & Gilbert, F., 1986. Observations of anomalous splitting and their interpretation in terms of aspherical structure, *J. geophys. Res.,* **91,** 10 203–10 228.

Ritzwoller, M., Masters, G. & Gilbert, F., 1988. Constraining aspherical structure with low frequency interaction coefficients: application to uncoupled multiplets, *J. geophys. Res.,* **93,** 6369–6396.

Romanowicz, B., Li, X-D. & Durek, J.J., 1996. Anisotropy in the inner core; could it be due to low-order convection?, *Science,* **274,** 963–966.

Shearer, P.M. & Toy, K.M., 1991. PKP(BC) and PKP(DF) differential travel times and aspherical structure of the Earth's inner core, *J. geophys. Res.,* **96,** 2233–2247.

Shearer, P.M., Toy, K.M. & Orcutt, J.A., 1988. Axi-symmetric Earth models and inner-core anisotropy, *Nature,* **333,** 228–232.

Smith, M.F. & Masters, G., 1989. Aspherical structure constraints from normal mode frequency and attenuation measurements, *J. geophys. Res.,* **94,** 1953–1976.

Souriau, A. & Romanowicz, B., 1996. Anisotropy in inner core attenuation; a new type of data to constrain the nature of the solid core, *Geophys. Res. Lett.,* **23,** 1–4.

Souriau, A. & Romanowicz, B., 1997. Anisotropy in the inner core; relation between P-velocity and attenuation, *Phys. Earth planet. Inter.,* **101,** 33–47.

Song, X., 1996. Anisotropy in the central part of the inner core, *J. geophys. Res.,* **101,** 16 089–16 097.

Song, X. & Helmberger, D.V., 1992. Velocity structure near the inner core boundary from waveform modeling, *J. geophys. Res.,* **97,** 6573–6586.

Song, X. & Helmberger, D.V., 1995. Depth dependence of anisotropy of Earth's inner core, *J. geophys. Res.,* **100,** 9805–9816.

Song, X. & Helmberger, D.V., 1998. Seismological evidence for an inner core transition zone, *EOS, Trans. Am. geophys. Un.,* **79,** s218 (abstract).

Song, X. & Richards, P.G., 1996. Seismological evidence for differential rotation of the Earth's inner core, *Nature,* **382,** 221–224.

Stacey, F.D., 1977. *Physics of the Earth*, 2nd edn, pp. 319–323, John Wiley, New York.

Stixrude, L. & Cohen, R.E., 1995. High-pressure elasticity of iron and anisotropy of Earth's inner core, *Science,* **267,** 1972–1975.

Su, W.-J. & Dziewonski, A.M., 1995. Inner core anisotropy in three dimensions, *J. geophys. Res.,* **100,** 9831–9852.

Su, W.-J., Dziewonski, A.M. & Jeanloz, R., 1996. Planet within a planet; rotation of the inner core of Earth, *Science,* **274,** 1883–1887.

Tanaka, S. & Hamaguchi, H., 1997. Degree one heterogeneity and hemispherical variation of anisotropy in the inner core from PKP(BC)-PKP(DF) times, *J. geophys. Res.,* **102,** 2925–2938.

Tanimoto, T., 1986. Free oscillations of a slightly anisotropic Earth *Geophys. J. R. astr. Soc.,* **87,** 493–517.

Tromp, J., 1993. Support for anisotropy of the Earth's inner core from free oscillations, *Nature,* **366,** 678–681.

Tromp, J., 1995a. Normal mode splitting observations from the great 1994 Bolivia and Kuril Islands earthquakes: constraints on the structure of the mantle and core, *GSA Today,* **5,** 137.

Tromp, J., 1995b. Normal-mode splitting due to inner-core anisotropy, *Geophys. J. Int.,* **121,** 963–968.

Tromp, J., 1996. Normal-mode constraints on the shear and bulk sound velocity of the mantle, *EOS, Trans. Am. geophys. Un.,* **77,** 483.

Vinnik, L., Romanowicz, B. & Breger, L., 1994. Anisotropy in the center of the inner core, *Geophys. Res. Lett.,* **21,** 1671–1674.

Widmer, R.W., Masters, G. & Gilbert, F., 1992. Observably split multiplets—data analysis and interpretation in terms of large-scale aspherical structure, *Geophys. J. Int.,* **111,** 559–576.

Wong, Y.K., 1989. Upper mantle heterogeneity from phase and amplitude data of mantle waves, *PhD thesis,* Harvard University, Cambridge, MA.

Woodhouse, J.H. & Dahlen, F.A., 1978. The effect of a general aspherical perturbation on the free oscillations of the Earth, *Geophys. J. R. astr. Soc.,* **53,** 335–354.

Woodhouse, J.H., Giardini, D. & Li, X.-D., 1986. Evidence for inner core anisotropy from free oscillations, *Geophys. Res. Lett.,* **13,** 1549–1552.